ISSN 1064-2269, Journal of Communications Technology and Electronics, 2015, Vol. 60, No. 7, pp. 707–736. © Pleiades Publishing, Inc., 2015.
Original Russian Text © V.F. Kravchenko, O.V. Kravchenko, Ya.Yu. Konovalov, V.I. Pustovoit, D.V. Churikov, 2015, published in Radiotekhnika i Elektronika, 2015, Vol. 60, No. 7, pp. 663–694.

REVIEW

Atomic, WA-Systems, and R-Functions Applied in Modern Radio Physics Problems: Part III

V. F. Kravchenko[a, b, c], O. V. Kravchenko[a, b], Ya. Yu. Konovalov[b], V. I. Pustovoit[b, c], and D. V. Churikov[a, c, d]

[a] *Kotel'nikov Institute of Radio Engineering and Electronics, Russian Academy of Sciences, Mokhovaya ul. 11, korp. 7, Moscow, 125009 Russia*

[b] *Bauman State Technical University, Vtoraya Baumanskaya ul. 5, Moscow, 105005 Russia*

[c] *Scientific and Technological Center of Unique Instrumentation, Russian Academy of Sciences, ul. Butlerova 15, Moscow, 117342 Russia*

[d] *Moscow Institute of Physics and Technology (State University), Institutskii per. 9, Dolgoprudnyi, Moscow oblast, 141700 Russia*

e-mail: kvf-ok@mail.ru, mpio_nice@mail.ru

Received December 15, 2014

Abstract—The third part of the review is devoted to the application of families of atomic functions for the construction of weighting functions (windows) based on convolutions that allow a decrease of the side-lobe level in the problems of nonparametric estimation of probability density and in the systems of phase locking with sampling.

DOI: 10.1134/S1064226915070104

1. PHYSICAL PROPERTIES OF THE $\mathrm{ch}_{a,n}(x)$ FAMILY OF ATOMIC FUNCTIONS

It is known from [1–16] that weighting functions (windows) based on atomic functions (AFs) are widely employed in digital signal processing (DSP) and images, tomography, radio astronomy, statistical processing, etc. In such problems [1–15, 17], main attention is paid to the following physical characteristics: highest side-lobe level (SLL), coherent gain (CG), worst case process loss (WCPL), and widths of window at levels of 3 and 6 dB. Relatively low SLL, high CG, and low MCL are needed. In accordance with uncertainty principle [9, 10], such requirements are contradictory. The proposed approach makes it possible to reach a compromise. For this purpose, we construct a multiple convolution [18] that exhibits a relatively low SLL in accordance with the properties of the Fourier transform and, then, perform its truncation for an increase in the CG and a decrease in the conversion loss. Note that convolutions of AFs [19–25, 29] represent AFs [1, 2] and can be found as solutions to the corresponding functional differential equations (FDE) in the absence of calculations of convolution.

1.1. Formulation of the Problem and the Method for Solution

We construct weighting function (WF) with a relatively low SLL and high CG as a product of two functions $f(kx)g(x)$, where $f(x)$ is the multiple convolution of AF the side lobes of which rapidly decrease with an increase in the order of convolution and functions $g(x)$ exhibits a relatively high CG. We study convolutions of AFs $\mathrm{h}_a(x)$ that form a two-parametric family of AFs $\mathrm{ch}_{a,n}(x)$ [19–25].

1.2. Main Properties of the Convolutions of AFs

We consider the convolution of two atomic functions $f(x)$ and $g(x)$ with identical scaling parameters a that are given by

$$f^{(n_f)} = \sum_{m=1}^{M} c_{f_m} f(ax - b_{f_m}), \tag{1}$$

$$g^{(n_g)} = \sum_{k=1}^{K} c_{g_k} f(ax - b_{g_k}). \tag{2}$$

Note that such a convolution exists as a convolution of two infinitely smooth functions with compact support. The Fourier transforms of Eqs. (1) fnd (2) represent equations for spectra of functions $F = \hat{f}$ and $G = \hat{g}$ written as

$$(it)^{n_f} F(t) = F\left(\frac{t}{a}\right) \sum_{m=1}^{M} \frac{c_{f_m}}{a} \exp\left(-\frac{itb_{f_m}}{a}\right), \tag{3}$$

$$(it)^{n_g} G(t) = G\left(\frac{t}{a}\right) \sum_{k=1}^{K} \frac{c_{g_k}}{a} \exp\left(-\frac{itb_{g_k}}{a}\right). \tag{4}$$

We multiply expressions (3) and (4) to obtain the equation for product of spectra $P(t) = F(t)G(t)$:

$$(it)^{n_f+n_g}P(t) = P\left(\frac{t}{a}\right)\sum_m\sum_k\frac{c_{f_m}c_{g_k}}{a^2}\exp\left(-\frac{it}{a}(b_{f_m}+b_{g_k})\right). \quad (5)$$

Using the inverse Fourier transform of this expression with allowance for the property $\frac{1}{a}\exp\left(\frac{ibt}{a}\right)F\left(\frac{t}{a}\right) \sim f(ax+b)$, we derive the equation for convolution $p(x) = f(x)*g(x)$:

$$p^{(n_f+n_g)} = \sum_m\sum_k\frac{c_{f_m}c_{g_k}}{a}p(ax-b_{f_m}-b_{g_k}). \quad (6)$$

This expression is similar to expression (1), so that resulting function $p(x)$ is classified as AF.

Using the explicit representation of function $p(x)$ (expression (6)), we can construct an iterative algorithm using the method of [20, 21] or employ a rapidly converging Fourier series.

Example 1. We consider self-convolution of function $\mathrm{h}_a(x)$ [13]. Using the above procedure, we derive the following equation:

$$y''(x) = \frac{a^3}{4}\big(y(ax+2)-2y(ax)+y(ax-2)\big). \quad (7)$$

After several repetitions of the procedure, we obtain an equation for the convolution of n functions $\mathrm{h}_a(x)$. Such a convolution is written as $\mathrm{ch}_{a,n}(x)$. Below, we prove the existence and study the main properties.

1.3. Definition of AF $\mathrm{ch}_{a,n}(x)$ *and Theorem of Existence*

Definition. AFs $\mathrm{ch}_{a,n}(x)$ are finite solutions to FDE

$$y^{(n)} = a^{n+1}2^{-n}\sum_{k=0}^{n}C_n^k(-1)^k y(ax+n-2k), \quad (8)$$
$$a>1,\quad n=1,2,3\ldots.$$

with the support $[-n/(a-1); n/(a-1)]$ that satisfy the normalization condition

$$\int_{-\infty}^{\infty}y(x)dx = 1.$$

Theorem. For each $n = 1,2,3,\ldots$ and $a > 1$, the FDE

$$y^{(n)} = l\sum_{k=0}^{n}C_n^k(-1)^k y(ax+n-2k) \quad (9)$$

has a single finite infinitely differentiable solution with support $[-n/(a-1); n/(a-1)]$ that satisfies the normalization condition $\int_{-\infty}^{\infty}y(x)dx = 1$. A necessary condition for the existence of solution is written as $l = a^{n+1}2^{-n}$.

Proof. We search for solution to Eq. (9) in space L_1 of functions that are summable at the entire axis. Using the Fourier transform of Eq. (9), we obtain

$$(it)^nF(t) = l\sum_{k=0}^{n}C_n^k(-1)^k\frac{1}{a}F\left(\frac{t}{a}\right)\exp\left(\frac{it}{a}(n-2k)\right), \quad (10)$$

where $F(t)$ is the Fourier transform of desired function $y(x)$. To simplify expression (10), we use the identity that follows from the Newton binomial:

$$\sum_{k=0}^{n}C_n^k(-1)^k\exp\left(\frac{it}{a}(n-2k)\right) = \left(\exp\left(\frac{it}{a}\right)-\exp\left(-\frac{it}{a}\right)\right)^n = 2^ni^n\sin^n\left(\frac{t}{a}\right). \quad (11)$$

Substituting expression (11) in formula (10), we derive

$$F(t) = l\frac{2^n}{a}F\left(\frac{t}{a}\right)\sin^n\left(\frac{t}{a}\right)\frac{1}{t^n} = l\frac{2^n}{a^{n+1}}F\left(\frac{t}{a}\right)\mathrm{sinc}^n\left(\frac{t}{a}\right).$$

Then, function $F(t)$ is represented as

$$F(t) = \prod_{k=1}^{\infty}l\frac{2^n}{a^{n+1}}\mathrm{sinc}^n\left(\frac{t}{a^k}\right). \quad (12)$$

Infinite product (12) converges if $l = 2^{-n}a^{n+1}$. Thus, we have

$$F(t) = \prod_{k=1}^{\infty}\mathrm{sinc}^n\left(\frac{t}{a^k}\right). \quad (13)$$

In accordance with the Paley–Wiener theorem, function $y(x)$ exists, can be found as $y(x) = \frac{1}{2\pi}\int_{-\infty}^{\infty}\exp(itx)F(t)dt$, and is zero outside segment $\left[-\frac{n}{a-1}; \frac{n}{a-1}\right]$. It follows from expression (13) that $\int_{-\infty}^{\infty}y(x)dx = 1$. Thus, the theorem is proven.

The notation for the resulting function is $\mathrm{ch}_{a,n}(x)$.

1.4. Main Properties of Family of AFs $\mathrm{ch}_{a,n}(x)$

Taking into account relationships $F(t) = \prod_{k=1}^{\infty}\mathrm{sinc}^n\left(\frac{t}{a^k}\right) = \left(\prod_{k=1}^{\infty}\mathrm{sinc}\left(\frac{t}{a^k}\right)\right)^n = \left(\hat{\mathrm{h}}_a(t)\right)^n$, we conclude that function $\mathrm{ch}_{a,n}(x)$ represents a convolution of n functions $\mathrm{h}_a(x)$. Therefore, AFs $\mathrm{up}(x)$, $\mathrm{h}_a(x)$, $\mathrm{cup}(x)$, and $\Xi_n(x)$ are particular cases of AF $\mathrm{ch}_{a,n}(x)$: $\mathrm{ch}_{2,1}(x) = \mathrm{up}(x)$, $\mathrm{ch}_{2,2} = \mathrm{cup}(x)$, $\mathrm{ch}_{a,1}(x) = \mathrm{h}_a(x)$, and $\mathrm{ch}_{n+1,n}(x) = \Xi_n(x)$. In this case, Eq. (8) coincides with the equation of the corresponding AF. In addition,

$\mathrm{ch}_{a,n}(x)$ can be considered as an infinite convolution of the Schoenberg B-splines of power $n-1$.

Below we prove several properties of AF $\mathrm{ch}_{a,n}(x)$.

(i) Function $\mathrm{ch}_{a,n}(x)$ is nonnegative as the convolution of nonnegative functions $\mathrm{h}_a(x)$.

(ii) Function $\mathrm{ch}_{a,n}(x)$ is an even function as the convolution of even functions.

(iii) In accordance with the conditions of the theorem of existence, we have

$$\int_{-\infty}^{\infty} \mathrm{ch}_{a,n}(x)dx = 1, \text{ a } \mathrm{supp}(\mathrm{ch}_{a,n}(x)) = \left[-\frac{n}{a-1}; \frac{n}{a-1}\right].$$

(iv) Upon periodic extension, AF $\mathrm{ch}_{a,n}(x)$ is represented using the following Fourier series:

$$\mathrm{ch}_{a,n}(x) = \frac{a-1}{n}\left(\frac{1}{2} + \sum_{k=1}^{\infty} F\left(\frac{a-1}{n}\pi k\right)\cos\left(\frac{a-1}{n}\pi kx\right)\right),$$

where $F(t) = \prod_{k=1}^{\infty} \mathrm{sinc}^n\left(\frac{t}{a^k}\right)$.

(v) An alternative method for the calculation of AF $\mathrm{ch}_{a,n}(x)$ employs an iterative algorithm based on the fact that function $\mathrm{ch}_{a,n}(x)$, which is the solution to Eq. (9), represents a fixed point of operator

$$A(y) = a^{n+1}2^{-n}I^n\left(\sum_{k=0}^{n} C_n^k(-1)^k y(ax+n-2k)\right),$$

where $I(y(x)) = \int_{-n/(a-1)}^{x} y(t)dt$.

Then, function $\mathrm{ch}_{a,n}(x)$ is the limit of a uniformly converging series $\{f_k(x)\}$, $f_k(x) = A(f_{k-1}(x))$. Several variants of the implementation of the algorithm can be found in [19–25].

(vi) Derivatives $\mathrm{ch}_{a,n}(x)$ of the order that is a multiple of n are calculated using self-substitution of expression (9).

(vii) The following convolution is valid: $\mathrm{ch}_{a,n}(x)*\mathrm{ch}_{a,m}(x) = \mathrm{ch}_{a,n+m}(x)$.

(viii) Shifts of AF $\mathrm{ch}_{a,n}(x)$ provide expansion of unity:

$$\frac{2}{a}\sum_{k\in\mathbb{Z}} \mathrm{ch}_{a,n}\left(x + \frac{2k}{a}\right) \equiv 1.$$

Proof. Using notation $S(x) = \sum_{k\in\mathbb{Z}} \mathrm{ch}_{a,n}\left(x + \frac{2k}{a}\right)$ and Eq. (9), we find that $S^{(n)}(x) \equiv 0$. Hence, $S(x)$ is a polynomial with an order of no greater than n. Note that $S(x)$ is a bounded function. Therefore, $S(x) \equiv S$ is the constant that is equal to $a/2$.

Shifted functions $\mathrm{ch}_{a,n}(x)$ can also be used to represent polynomials with a degree of no greater than $n-1$. The corresponding proof is similar to the above proof. Exact representation of polynomials using shifted functions $\mathrm{ch}_{a,n}(x)$ can be employed for efficient interpolation of smooth functions. The algorithms for the 1D and 2D interpolations using shifted AFs $\mathrm{ch}_{a,n}(x)$ can be found in [24, 25].

(ix) A useful property of AFs is related to the fact that their moments are calculated with the aid of recursion relations in the absence of integration.

We construct recursion relations for the moments of $\mathrm{ch}_{a,2}$. It is known that the moments of function are related to the coefficients of the expansion of the Fourier transform of the function in the Taylor series

$$\int_{-2/(a-1)}^{2/(a-1)} x^{2m}\,\mathrm{ch}_{a,2} = (-1)^m(2m)!c_{2m}.$$

The Fourier transform of function $\mathrm{ch}_{a,2}$ is given by expression (13). The following equality is valid:

$$F(t) = \mathrm{sinc}^2\left(\frac{t}{a}\right)F\left(\frac{t}{a}\right). \tag{14}$$

This expression can be expanded in the Taylor series at point $t_0 = 0$. For this purpose, we represent $\mathrm{sinc}^2(t/a)$ as

$$\mathrm{sinc}^2\left(\frac{t}{a}\right) = \frac{\sin^2\left(\frac{t}{a}\right)}{\left(\frac{t}{a}\right)^2} = \frac{1-\cos\left(\frac{2t}{a}\right)}{2\left(\frac{t}{a}\right)^2}$$
$$= \sum_{k=0}^{\infty}\frac{(-1)^k\left(\frac{2t}{a}\right)^{2k+2}}{(2k+2)!2\left(\frac{t}{a}\right)^2} = \sum_{k=0}^{\infty}\frac{(-1)^k 2^{2k+1}t^{2k}}{(2k+2)!a^{2k}}.$$

Fourier transform (13) is an even function, so that coefficients of even powers of t differ from zero and expression (14) is represented as

$$\sum_{n=0}^{\infty} c_{2n}t^{2n} = \sum_{l=0}^{\infty}\frac{(-1)^l 2^{2l+1}t^{2l}}{(2l+2)!a^{2l}}\sum_{k=0}^{\infty}\frac{c_{2k}t^{2k}}{a^{2k}}. \tag{15}$$

We assume that the coefficients of t^{2n} are equal to each other (in the right-hand side of expression (15), we use $l = n-k$):

$$c_{2n}t^{2n} = \sum_{k=0}^{n}\frac{(-1)^{n-k}2^{2n-2k+1}t^{2n-2k}c_{2k}t^{2k}}{(2n-2k+2)!a^{2n-2k}a^{2k}}.$$

Term c_{2n} in the right-hand side is written as

$$c_{2n} = \sum_{k=0}^{n} \frac{(-1)^{n-k} 2^{2n-2k+1} c_{2k}}{(2n-2k+2)!\, a^{2n}}$$
$$= \sum_{k=0}^{n-1} \frac{(-1)^{n-k} 2^{2n-2k+1} c_{2k}}{(2n-2k+2)!\, a^{2n}} + \frac{2c_{2n}}{2a^{2n}}.$$

Thus, we obtain

$$c_{2n} = \frac{1}{a^{2n}-1} \sum_{k=0}^{n-1} \frac{(-1)^{n-k} 2^{2n-2k+1} c_{2k}}{(2n-2k+2)!}.$$

Using the expansion of functions $\mathrm{sinc}^n(t/a)$ in the Taylor series, we derive the moments of function $\mathrm{ch}_{a,n}(x)$ for each n. In particular, the relationship for $n = 3$, is written as

$$\int_{-3/(a-1)}^{3/(a-1)} x^{2m}\, \mathrm{ch}_{a,3} = (-1)^m (2m)!\, c_{2m},$$

where

$$c_{2m} = \frac{1}{a^{2m}-1} \sum_{k=0}^{m-1} \frac{(-1)^{m-k} \left(3^{2m-2k+1}-1\right) 3c_{2k}}{4(2m-2k+2)!}.$$

For the corresponding parameters a and n, the above formulas coincide with the known expression of [5, 13] for moments of AFs $\mathrm{up}(x)$, $\mathrm{h}_a(x)$, and $\Xi_n(x)$.

1.5. A New Class of WFs and Its Main Properties

The application of the convolutions of AFs in DSP has been proposed in [3, 4]. Using new family $\mathrm{ch}_{a,n}(x)$, we can generalize several results of [3, 4]. For this purpose, we study new structures of WFs (windows) $w_{a,n}(t) = \mathrm{ch}_{a,n}(st)/\mathrm{ch}_{a,n}(0)$, where factor $s = (a-1)/n$ reduces the function to support $[-1, 1]$. In accordance with the approach of [1–15, 17], we used the following physical characteristics in the analysis of the physical properties.

(i) Highest SLL (HSLL) (dB)

$$k_1 = -20 \log \max_k \left|W(\omega_k)/W(0)\right|,$$

where ω_k are the points of local maxima of the spectrum of window except for $\omega_0 = 0$.

(ii) Coherent gain

$$k_2 = \frac{1}{2} \int_{-1}^{1} w(t)dt.$$

(iii) Equivalent noise bandwidth (ENBW)

$$k_3 = 2 \int_{-1}^{1} w^2(t)dt \Bigg/ \left(\int_{-1}^{1} w(t)dt \right)^2.$$

(iv) Bandwidth at a level of 3 dB $k_4 = 2\omega$, where ω is the maximum frequency that satisfies equality $-20 \log \left|W(\omega)/W(0)\right| = 3$.

(v) Scallop loss (SL, dB)

$$k_5 = -20 \log \left| W\left(\frac{\pi}{2}\right) \Big/ W(0) \right|.$$

(vi) Worst case process loss (dB)

$$k_6 = 10 \log k_3 + k_5.$$

(vii) Bandwidth at a level of 6 dB $k_7 = 2\omega$, where ω is the maximum frequency that satisfies equality $-20 \log \left|W(\omega)/W(0)\right| = 6$.

(viii) Overlap correlation (%) for the 75% (k_8) and 50% (k_9) overlapping

$$k_8 = \int_{-0.5}^{1} w(t)w(t-0.5)dt \Bigg/ \int_{-1}^{1} w^2(t)dt,$$

$$k_9 = \int_{0}^{1} w(t)w(t-1)dx \Bigg/ \int_{-1}^{1} w^2(t)dx.$$

Expression (13) (the Fourier transform of AF $\mathrm{ch}_{a,n}(t)$) shows that an increase in n leads to a rapid decrease in the SLL and an increase in the width of the central lobe. On the other hand, function $\mathrm{ch}_{a,n}(t)$ is concentrated at the center of the support and rapidly decreases at the ends when n increases. This circumstance leads to a decrease in the signal power owing to undesired suppression of the samples of the signal under study at the edges. In this case, CG and MCL become worse. In this regard, it is expedient to consider the effective support for AF $\mathrm{ch}_{a,n}(x)$, which can be determined as

$$\int_{S_e} \mathrm{ch}_{a,n}(t)dt \Bigg/ \int_{R} \mathrm{ch}_{a,n}(t)dt = 99.99\%.$$

Note that the truncation of $w_{a,n}(t)$ to the effective support leads to a certain increase in the SLL, since the spectrum of the truncated function represents a convolution of the compressed spectrum of original function and the spectrum of rectangular window $\mathrm{sinc}(\omega)$. However, the SLL of the truncated window is acceptable, since the SLL of $w_{a,n}(t)$ is extremely low. At the same time, the truncation makes it possible to reduce the power loss due to an increase in the CG. The broadening of the WF in time domain leads to the proportional narrowing of the spectrum and the corresponding decrease in the width of the central lobe. This circumstance leads to significant improvement of the physical characteristics of the window. Table 1 presents the physical parameters of WFs (windows) $w_{a,n}(t)$ that are truncated to the effective support.

The CGs in Table 1 are approximately equal and close to 0.5, since the WFs are reduced to the effective support. Note that the SLL decreases with an increase

Table 1. Physical characteristics of WFs (windows) $w_{a,n}(kt)$

a	n	k	HSLL	CG	ENBW	k_4	SL	WCPL	k_7	k_8	k_9
Multiple convolutions $h_{1.5}(t)$											
1.5	1	0.6510	−35.4	0.53	1.39	1.33	1.67	3.10	1.85	69.83	21.91
	2	0.4844	−48.9	0.48	1.49	1.42	1.48	3.21	1.98	65.61	17.28
	3	0.4010	−48.6	0.47	1.52	1.44	1.43	3.25	2.02	64.34	16.12
Multiple convolutions $up(t)$											
2	2	0.6080	−42.0	0.51	1.43	1.36	1.58	3.15	1.91	67.96	19.76
	3	0.5100	−47.9	0.49	1.49	1.41	1.49	3.21	1.97	65.74	17.42
	4	0.4466	−48.6	0.48	1.51	1.43	1.45	3.24	2.00	64.74	16.48
Multiple convolutions $h_{2.5}(t)$											
2.5	2	0.6748	−35.9	0.52	1.40	1.33	1.66	3.11	1.85	69.50	21.62
	3	0.5722	−45.8	0.50	1.47	1.39	1.52	3.19	1.95	66.62	18.33
	4	0.5032	−48.6	0.48	1.50	1.42	1.47	3.22	1.98	65.32	17.02
Multiple convolutions $h_3(t)$											
3	3	0.6136	−43.7	0.50	1.45	1.38	1.55	3.17	1.93	67.19	18.95
	4	0.5416	−48.7	0.48	1.49	1.41	1.48	3.21	1.98	65.66	17.35
	5	0.4886	−48.5	0.48	1.51	1.43	1.45	3.23	2.00	64.88	16.60
Multiple convolutions $h_{3.5}(t)$											
3.5	3	0.6436	−42.2	0.51	1.44	1.37	1.57	3.16	1.91	67.57	19.38
	4	0.5694	−48.3	0.49	1.48	1.41	1.49	3.21	1.97	65.89	17.58
	5	0.5140	−48.5	0.48	1.50	1.42	1.46	3.23	1.99	65.06	16.77

in the order of convolution and the WCPL is no greater than 3.3. A disadvantage of the truncated windows is related to the discontinuities at the ends that can be smoothed using an additional WF. We consider combination windows represented as $\tilde{w}(t) = w_{a,n}(kt)w(t)$, where k is the factor that determines the broadening of the function for truncation to the effective support and $w(t)$ is the WF. The spectrum of such a window is represented as the convolution

$$\tilde{W}(\omega) = W_{a,n}\left(\frac{\omega}{k}\right) * W(\omega).$$

The effective support is determined by factor k.

Table 2 presents the characteristics of the combination windows that represent products of windows from Table 1 and the Hanning windows. The corresponding CGs are lower (close to 0.41) and the HSLL rapidly decreases. Table 3 shows the windows that result from the truncation of $w_{a,n}(t)$ by window $\cos^2(\pi t/2)$, The corresponding CGs are close to 0.36. Note that the frequency response function of $w_{a,n}(kt)$ has a distinct structure with developed side lobes whereas the combination windows truncated with the Hanning windows exhibit broadening and merging of side lobes and the partial merging of the side lobes and main lobe. The effect becomes stronger when the power of the cosine function increases.

The CGs of windows $w(t)$ must be relatively high, since the truncation is aimed at a decrease in the energy loss. Several classical windows (Hamming, Riemann, and Riesz windows) serve as $w(t)$.

Tables 4–6 present the characteristics of the resulting windows. Figures 1 and 2 illustrate the effect of function $w(t)$ on the window shape and frequency response function.

In addition to function $\mathrm{ch}_{a,n}$, we consider AF fup_n [1, 2, 5–7], which exhibits reasonable HSLL. In spite of the fact that the side lobes of function $\mathrm{ch}_{a,n}$ are lower, function fup_n, which represents a solution to the first-order equation, requires a lower amount of computations. This circumstance accounts for the practical interest in the windows based on AF fup_n.

For the construction of the windows based on AF fup_n, we employ the above approach and study the behavior of windows

$$\tilde{w}(t) = fup_n\left(\frac{2kt}{n+2}\right)w(t), \tag{16}$$

Table 2. Physical characteristics of combination WFs (windows) $w_{a,n}(kt)\cos(\pi t/2)$

n	HSLL	CG	ENBW	k_4	SL	WCPL	k_7	k_8	k_9	k
Multiple convolutions $h_{1.5}(t)$ truncated with window $\cos(t)$										
2	–65.1	0.41	1.77	1.67	1.06	3.53	2.34	55.01	8.02	0.4844
3	–67.9	0.40	1.80	1.70	1.02	3.57	2.38	53.82	7.41	0.4010
4	–68.0	0.40	1.81	1.71	1.01	3.59	2.40	53.26	7.14	0.3494
Multiple convolutions $up(t)$ truncated with window $\cos(t)$										
2	–49.1	0.42	1.71	1.63	1.12	3.46	2.27	57.15	9.33	0.6080
3	–64.4	0.41	1.76	1.67	1.06	3.52	2.34	55.11	8.09	0.5100
4	–68.2	0.40	1.79	1.69	1.03	3.56	2.37	54.18	7.59	0.4466
Multiple convolutions $h_{2.5}(t)$ truncated with window $\cos(t)$										
3	–57.8	0.42	1.74	1.65	1.08	3.50	2.32	55.90	8.55	0.5722
4	–68.3	0.41	1.77	1.68	1.05	3.54	2.35	54.72	7.87	0.5032
5	–67.7	0.40	1.79	1.70	1.03	3.56	2.38	54.06	7.53	0.4536
Multiple convolutions $h_3(t)$ truncated with window $\cos(t)$										
3	–53.3	0.42	1.73	1.64	1.09	3.48	2.30	56.41	8.86	0.8282
4	–63.7	0.41	1.77	1.67	1.06	3.53	2.34	55.02	8.04	0.8192
5	–67.2	0.40	1.78	1.69	1.04	3.55	2.37	54.31	7.66	0.8152
Multiple convolutions $h_{3.5}(t)$ truncated with window $\cos(t)$										
3	–50.6	0.42	1.72	1.63	1.10	3.47	2.29	56.74	9.06	0.8310
4	–62.2	0.41	1.76	1.67	1.06	3.52	2.34	55.23	8.16	0.8206
5	–66.6	0.41	1.78	1.69	1.04	3.55	2.36	54.47	7.75	0.8160

where k is the factor that reduces the function to the effective support. Table 7 presents the physical characteristics of the windows that are calculated with the aid of formula (16). The Hamming, Riemann, and Riesz windows serve as $w(t)$.

As distinct from the structure of [1, 3–5], we consider expression (16) in which coefficient k provides the reduction of the AF family to effective support. Thus, we obtain minimum energy loss and reasonable HSLL. The comparison of the physical results shows that the WFs (windows) under study exhibit low loss levels and make it possible to work with weak signals whereas the Kravchenko windows provide more accurate reconstruction of spectra of processed signals and exhibit extremely low SLL.

2. NONPARAMETRIC ESTIMATION OF PROBABILITY DENSITY BASED ON THE AF FAMILY

The topicality of nonparametric estimations [13–15, 26–36] in physical applications is related to the simplicity of structure and application in the scenarios in which the reconstructed quantity is unknown. Therefore, a new mathematical procedure of the nonparametric statistics that is obtained with the aid of the AF theory will make it possible to estimate the characteristics of the sequences under study in the absence of the a priori parametric information.

2.1. Nonparametric Estimation of the Probability Density Function of a Random Series

Let $X_1, X_2, \ldots, X_n$ be a sample of n independent observations of random quantity X with unknown probability density function (PDF) $f(x)$. Nonparametric estimation [28–36] is given by

$$f_n(x) = \frac{1}{nm}\sum_{j=1}^{n} K\left(\frac{X_j - x}{m}\right), \tag{17}$$

where $m = m(n)$ is a series of positive integers. In this case, we have $\lim_{n\to\infty} m(n) = 0$ and $K(x)$ is an even function that satisfies the normalization condition $\int_{-\infty}^{\infty} K(x)dx = 1$ and $K(x) \in L_2$. WF $K(x)$ is a feasible WF if its Fourier transform (FT) is nonnegative and no greater than unity for all real frequencies. Then, the following definition is possible.

Definition. A nonparametric problem of estimation of unknown distributions involves a search for a procedure that makes it possible to estimate nonparametrized distributions from a certain class of distributions.

The first moments of function H of statistics x_n are found as the moments of the limiting distribution of estimation (mean, variance, RMS deviation) under weak convergence and the following theorem is valid.

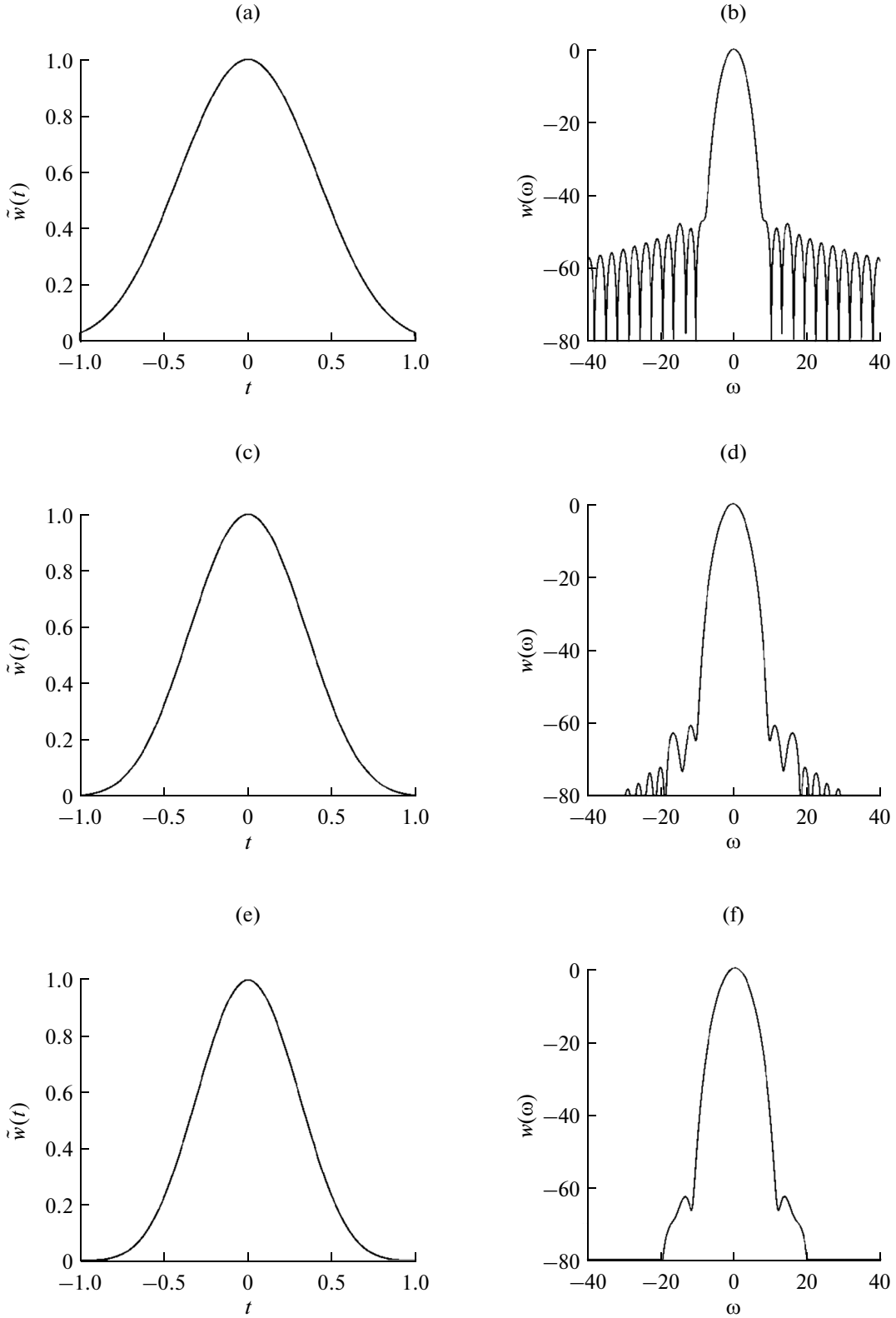

Fig. 1. (a), (c), and (e) Combination window $w_{4,4}(kt)w(t)$ and (b), (d), and (f) its frequency response functions for (a) and (b) rectangular, (c) and (d) $\cos(\pi t/2)$, and (e) and (f) $\cos^2(\pi t/2)$ windows $w(t)$.

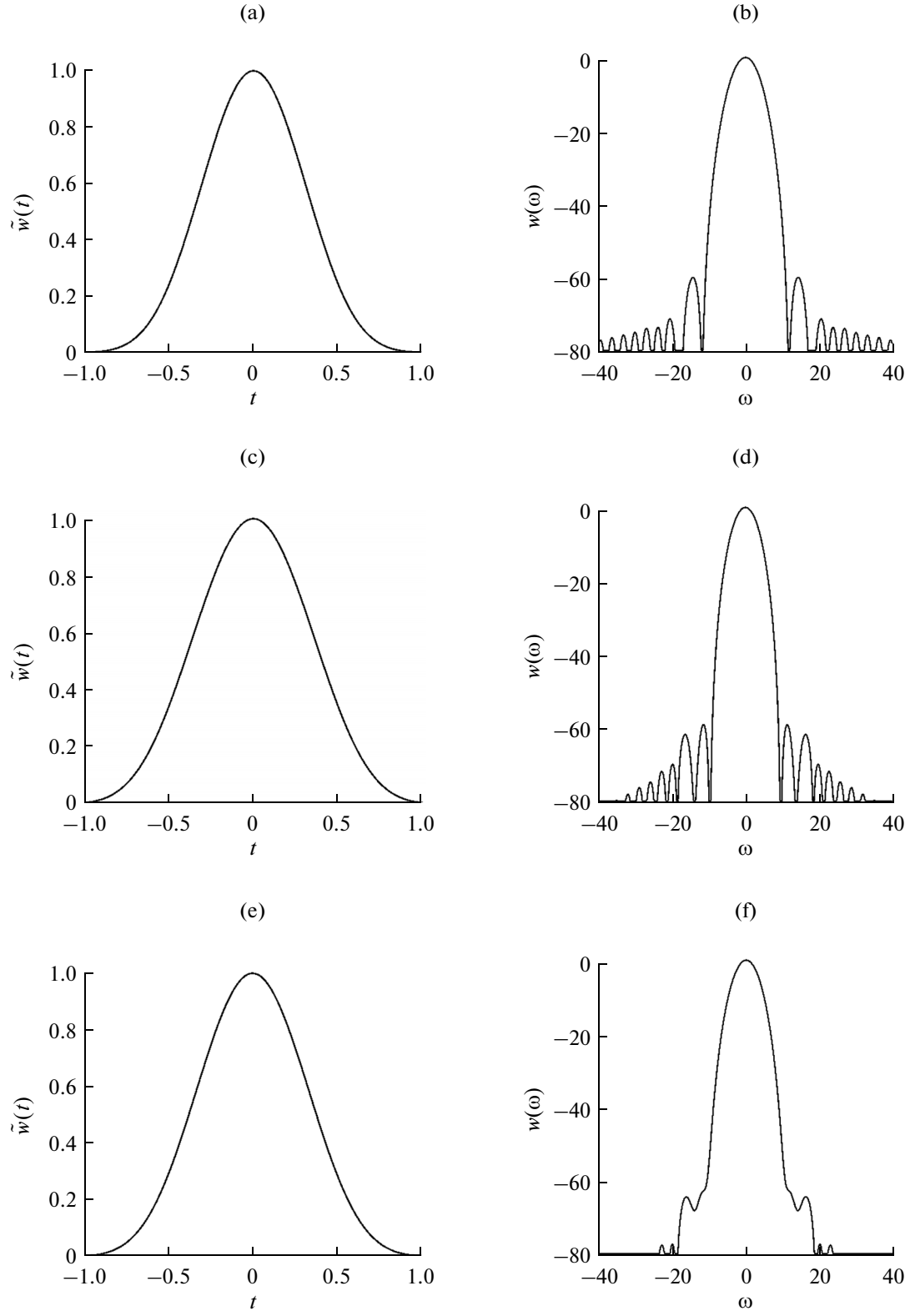

Fig. 2. (a), (c), and (e) Combination windows $w_{4,4}(kt)w(t)$ and (b), (d), and (f) frequency response functions for (a) and (b) Hamming, (c) and (d) Riesz, and (e) and (f) Riemann windows $w(t)$.

Table 3. Physical characteristics of combination WFs (windows) $w_{a,n}(kt)\cos^2(\pi t/2)$

n	HSLL	CG	ENBW	k_4	SL	WCPL	k_7	k_8	k_9	k
Multiple convolutions $h_{1.5}(t)$ truncated with window $\cos^2(t)$										
1	−48.4	0.39	1.89	1.79	0.92	3.68	2.51	50.53	5.25	0.6510
2	−75.5	0.36	1.99	1.88	0.83	3.82	2.64	46.58	3.89	0.4844
3	−80.0	0.36	2.02	1.91	0.81	3.86	2.68	45.52	3.57	0.4010
Multiple convolutions $up(t)$ truncated with window $\cos^2(t)$										
2	−54.0	0.37	1.94	1.84	0.87	3.76	2.58	48.43	4.56	0.6080
3	−74.7	0.36	1.99	1.88	0.84	3.82	2.64	46.67	3.92	0.5100
4	−80.0	0.36	2.01	1.90	0.82	3.85	2.67	45.84	3.66	0.4466
Multiple convolutions $h_{2.5}(t)$ truncated with window $\cos^2(t)$										
2	−80.0	0.37	1.91	1.81	0.90	3.72	2.54	49.45	5.04	0.6748
3	−59.6	0.37	1.97	1.86	0.85	3.79	2.62	47.37	4.15	0.5722
4	−73.9	0.36	2.00	1.89	0.83	3.83	2.65	46.32	3.81	0.5032
Multiple convolutions $h_3(t)$ truncated with window $\cos^2(t)$										
2	−70.2	0.37	1.90	1.79	0.92	3.70	2.52	50.03	5.38	0.7618
3	−53.6	0.37	1.96	1.85	0.86	3.78	2.60	47.82	4.30	0.7428
4	−68.6	0.36	1.99	1.88	0.83	3.82	2.64	46.59	3.89	0.7344
Multiple convolutions $h_{3.5}(t)$ truncated with window $\cos^2(t)$										
2	−80.0	0.37	1.89	1.78	0.93	3.69	2.50	50.40	5.61	0.7670
3	−50.3	0.37	1.95	1.85	0.87	3.77	2.59	48.11	4.40	0.7452
4	−65.0	0.36	1.99	1.88	0.84	3.82	2.63	46.78	3.95	0.7354

Theorem. If a distribution of a series of s-dimensional random values converges at $n \to \infty$ to the s-dimensional normal distribution $\mathrm{N}_s\{\mu,\sigma\}$ with a vector of mean values $\mu = (\mu_1,\ldots,\mu_s)$ and covariation matrix σ $(0 < \sigma_{jj} = \sigma_{jj}(x) < \infty,\ j = \overline{1,s})$, i.e., $d_n(x_n - x) \Rightarrow \mathrm{N}_s\{\mu,\sigma\}$, $H(x) \in \mathcal{N}_{1,s}$, and $\nabla H(x) \neq 0$), we obtain

$$d_n(H(x_n) - H(x)) \Rightarrow \mathrm{N}_1\left\{\sum_{j=1}^{s} H_j(x)\mu_j, \sum_{j,p=1}^{s} H_j(x)H_p(x)\sigma_{j,p}\right\}$$
$$= \mathrm{N}_1\left\{\nabla H(x)\mu^{\mathrm{T}}, \nabla H(x)\sigma\nabla^{\mathrm{T}}H(x)\right\}.$$

Here, $\mathcal{N}_{\nu,s}$ is the class of functions that have all of partial derivatives up to the ν-th order and $d_n \to \infty$. We assume that $\nabla^2 H(x)$ is the matrix of the second derivatives with elements $\left.\dfrac{\partial^2 H(z)}{\partial z_i \partial z_j}\right|_{z=x}$, $i,j = 1,\ldots,s$; $\eta = (\eta_1,\ldots,\eta_s)$ is the s-dimensional random quantity, X^2 is the 1D random quantity that has χ^2 distribution with a single degree of freedom, and N is the random quantity that is distributed in accordance with the standard normal law $\mathrm{N}_1\{0,1\}$. Three scenarios are possible.

(i) If $d_n(x_n - x) \Rightarrow \eta = (\eta_1,\ldots,\eta_s)$, and $H(x) \in \mathcal{N}_{1,s}$, $\nabla H(x) \neq 0$, then we have

$$d_n(H(x_n) - H(x)) \Rightarrow \sum_{j=1}^{s} H_j(x)\eta_j = \nabla H(x)\eta^{\mathrm{T}}.$$

(ii) If $d_n(x_n - x) \Rightarrow \eta = (\eta_1,\ldots,\eta_s)$, $H(x) \in \mathcal{N}_{2,s}$, $\nabla H(x) = 0$, and $\nabla^2 H(x) \neq 0$, then we have

$$d_n^2(H(x_n) - H(x))$$
$$\Rightarrow \frac{1}{2}\sum_{i,j=1}^{s} H_{i,j}(x)\eta_i\eta_j = \frac{1}{2}\eta\nabla^2 H(x)\eta^{\mathrm{T}}.$$

(iii) If $d_n(x_n - x) \Rightarrow \mathrm{N}_s\{0, I_s\}$, where I_s is the s-order unit diagonal matrix, then $d_n^2(H(x_n) - H(x))$ converges with respect to distribution to a sum of

Table 4. Physical characteristics of combination WFs (windows) truncated with the Hamming window

n	HSLL	CG	ENBW	k_4	SL	WCPL	k_7	k_8	k_9	k
Multiple convolutions $h_{1.5}(t)$ truncated with the Hamming window										
1	−50.1	0.40	1.82	1.73	0.99	3.60	2.42	52.82	6.76	0.6510
2	−68.0	0.37	1.93	1.82	0.90	3.75	2.56	48.66	5.04	0.4844
3	−69.8	0.37	1.96	1.84	0.88	3.79	2.60	47.54	4.63	0.4010
Multiple convolutions $up(t)$ truncated with the Hamming window										
2	−56.1	0.38	1.88	1.77	0.95	3.68	2.49	50.64	5.89	0.6080
3	−65.1	0.37	1.92	1.82	0.90	3.75	2.55	48.76	5.08	0.5100
4	−69.2	0.37	1.95	1.84	0.88	3.78	2.58	47.88	4.75	0.4466
Multiple convolutions $h_{2.5}(t)$ truncated with the Hamming window										
2	−69.9	0.39	1.84	1.74	0.98	3.64	2.45	51.78	6.53	0.6748
3	−56.6	0.38	1.91	1.80	0.92	3.72	2.53	49.51	5.38	0.5722
4	−66.8	0.37	1.93	1.82	0.89	3.76	2.57	48.38	4.94	0.5032
Multiple convolutions $h_3(t)$ truncated with the Hamming window										
2	−68.1	0.39	1.83	1.72	1.00	3.62	2.42	52.45	6.98	0.8114
3	−51.9	0.38	1.89	1.79	0.93	3.70	2.51	49.98	5.58	0.7882
4	−63.9	0.37	1.93	1.82	0.90	3.75	2.56	48.67	5.05	0.7770
Multiple convolutions $h_{3.5}(t)$ truncated with the Hamming window										
2	−64.7	0.39	1.81	1.71	1.02	3.60	2.40	52.89	7.30	0.8184
3	−49.0	0.38	1.88	1.78	0.94	3.69	2.50	50.30	5.72	0.7914
4	−61.6	0.37	1.92	1.81	0.90	3.74	2.55	48.87	5.13	0.7786

Table 5. Physical characteristics of combination WFs (windows) truncated with the Riemann window

n	HSLL	CG	ENBW	k_4	SL	WCPL	k_7	k_8	k_9	k
Multiple convolutions $h_{1.5}(t)$ truncated with the Riemann window										
1	−46.2	0.42	1.73	1.64	1.09	3.47	2.30	56.64	8.79	0.6510
	−74.3	0.39	1.83	1.73	0.98	3.62	2.43	52.41	6.60	0.4844
3	−72.3	0.39	1.86	1.76	0.96	3.66	2.47	51.25	6.08	0.4010
Multiple convolutions $up(t)$ truncated with the Riemann window										
2	−50.6	0.40	1.78	1.69	1.04	3.54	2.36	54.49	7.69	0.6080
3	−67.5	0.39	1.83	1.73	0.99	3.61	2.43	52.51	6.65	0.5100
4	−72.8	0.39	1.85	1.75	0.97	3.64	2.46	51.60	6.23	0.4466
Multiple convolutions $h_{2.5}(t)$ truncated with the Riemann window										
2	−41.9	0.41	1.75	1.66	1.08	3.50	2.32	55.73	8.50	0.6748
3	−59.4	0.40	1.81	1.71	1.01	3.59	2.41	53.29	7.03	0.5722
4	−71.6	0.39	1.84	1.74	0.98	3.63	2.44	52.13	6.47	0.5032
Multiple convolutions $h_3(t)$ truncated with the Riemann window										
3	−54.3	0.40	1.80	1.70	1.02	3.57	2.39	53.78	7.29	0.6136
4	−68.6	0.39	1.83	1.73	0.98	3.62	2.43	52.43	6.61	0.5416
5	−71.3	0.39	1.85	1.75	0.97	3.64	2.46	51.72	6.29	0.4886
Multiple convolutions $h_{3.5}(t)$ truncated with the Riemann window										
3	−51.2	0.41	1.79	1.70	1.03	3.56	2.38	54.10	7.46	0.6436
4	−66.2	0.39	1.83	1.73	0.99	3.61	2.42	52.63	6.71	0.5694
5	−70.4	0.39	1.85	1.75	0.97	3.63	2.45	51.89	6.36	0.5140

Table 6. Physical characteristics of combination WFs (windows) truncated with the Riesz window

n	HSLL	CG	ENBW	k_4	SL	WCPL	k_7	k_8	k_9	k
Multiple convolutions $h_{1.5}(t)$ truncated with the Riesz window										
2	–62.5	0.42	1.73	1.64	1.10	3.48	2.30	56.49	8.93	0.4844
3	–65.6	0.41	1.76	1.67	1.07	3.52	2.34	55.29	8.26	0.4010
4	–65.7	0.41	1.77	1.68	1.05	3.54	2.35	54.73	7.96	0.3494
Multiple convolutions $up(t)$ truncated with the Riesz window										
2	–48.0	0.43	1.68	1.59	1.16	3.41	2.23	58.66	10.37	0.6080
3	–62.5	0.42	1.73	1.64	1.10	3.47	2.29	56.59	9.00	0.5100
4	–65.7	0.41	1.75	1.66	1.08	3.51	2.32	55.66	8.46	0.4466
Multiple convolutions $h_{2.5}(t)$ truncated with the Riesz window										
3	–56.7	0.43	1.71	1.62	1.12	3.45	2.27	57.40	9.51	0.5722
4	–62.9	0.42	1.74	1.65	1.09	3.49	2.31	56.20	8.77	0.5032
5	–65.4	0.41	1.75	1.66	1.07	3.51	2.33	55.54	8.39	0.4536
Multiple convolutions $h_3(t)$ truncated with the Riesz window										
3	–52.6	0.43	1.69	1.61	1.14	3.43	2.25	57.91	9.85	0.8398
4	–61.6	0.42	1.73	1.64	1.10	3.48	2.30	56.51	8.96	0.8310
5	–63.0	0.41	1.75	1.65	1.08	3.50	2.32	55.79	8.53	0.8272
Multiple convolutions $h_{3.5}(t)$ truncated with the Riesz window										
3	–50.0	0.43	1.69	1.60	1.15	3.42	2.24	58.24	10.08	0.8424
4	–60.2	0.42	1.72	1.63	1.11	3.47	2.29	56.72	9.09	0.8324
5	–63.3	0.41	1.74	1.65	1.08	3.50	2.31	55.95	8.63	0.8280

Table 7. Physical characteristics of combination WFs (17)

n	HSLL	CG	ENBW	k_4	SL	WCPL	k_7	k_8	k_9	k
$fup_n(t)$ truncated with the Hamming window										
1	–59.0	0.39	1.84	1.73	0.99	3.63	2.43	52.08	6.71	0.7376
2	–51.7	0.38	1.89	1.78	0.93	3.70	2.51	50.09	5.63	0.6852
3	–62.1	0.37	1.92	1.81	0.91	3.74	2.55	48.92	5.14	0.6358
$fup_n(t)$ truncated with the Riesz window										
1	–40.0	0.44	1.63	1.55	1.22	3.35	2.17	60.36	11.74	0.7376
2	–52.4	0.43	1.69	1.61	1.14	3.43	2.25	58.02	9.93	0.6852
3	–60.1	0.42	1.72	1.63	1.11	3.47	2.29	56.77	9.12	0.6358
$fup_n(t)$ truncated with the Riemann window										
1	–41.5	0.41	1.74	1.65	1.09	3.49	2.31	56.06	8.73	0.7376
2	–54.5	0.40	1.80	1.70	1.02	3.56	2.38	53.89	7.35	0.6852
3	–67.0	0.39	1.83	1.73	0.99	3.61	2.42	52.68	6.73	0.6358

weighted sums s of random quantities X^2 and $s(s-1)$ is the product of independent standard normal random quantities (i.e., $H(x) \in \mathcal{N}_{2,s}$, $\nabla H(x) = 0$, and $\nabla^2 H(x) \neq 0$). Then, we have

$$d_n^2(H(x_n) - H(x))$$
$$\Rightarrow \frac{1}{2}\sum_{j=1}^{s} H_{j,j}(x) X_j^2 + \frac{1}{2}\sum_{i \neq j}^{s} H_{i,j}(x) N_i N_j.$$

Integral RMS error given by

$$E = \left\langle \int_{-\infty}^{\infty} (f_n(x) - f(x))^2 dx \right\rangle$$

serves as the quality criterion for estimation $f_n(x)$. The angular brackets denote ensemble averaging. For the feasible WF, the integral RMS error of the corresponding estimation cannot be simultaneously decreased for all of probability densities $f(x)$.

2.2. Feasible Estimations of the PDF and Its Derivatives

Using an example of AF $\mathrm{h}_a(x)$, we consider the construction of feasible WFs. It is known from [1, 5] that AFs $\mathrm{h}_a(x)$ $(a > 1)$ are finite solutions to the functional differential equation

$$y'(x) = \frac{a^2}{2}(y(ax+1) - y(ax-1)).$$

The main properties of AF $h_a(x)$ are as follows:

(i) $\mathrm{h}_a(x) = 0 = 0$ at $|x| \geq (a-1)^{-1}$;

(ii) $\mathrm{h}_a(x) = a/2$ at $|x| \leq \dfrac{a-2}{a(a-1)}$, $a \geq 2$;

(iii) Fourier transform of function $\mathrm{h}_a(x)$, which is represented as $\varphi_a(\omega) = \prod_{k=1}^{\infty} \dfrac{\sin(\omega/a^k)}{\omega/a^k}$, is zero at points $\omega = 2\pi n$, $n \neq 0$. If ω is relatively low in the numerical calculations, we may consider few terms of the product, since they rapidly tend to 1 when k increases.

Using the third property, we may represent function $\mathrm{h}_a(x)$ at interval $x \in \left[\dfrac{-1}{(a-1)}, \dfrac{1}{(a-1)}\right]$ as $\mathrm{h}_a(x) = (a-1)\left(\dfrac{1}{2} + \sum_{k=1}^{\infty} \varphi_a((a-1)\pi k) \cos((a-1)\pi k x)\right)$.

We consider function $\mathrm{ch}_a(x) = \mathrm{h}_a(x) * \mathrm{h}_a(x)$ that represents self-convolution of AF $\mathrm{h}_a(x)$. Function $\mathrm{h}_a(x)$ is an infinitely differentiable even function with support $\left[\dfrac{-2}{(a-1)}, \dfrac{2}{(a-1)}\right]$. After $l-1$ convolutions, we obtain function $\mathrm{ch}_{a,l}(x) = \dfrac{1}{2\pi}\int_{-\infty}^{\infty} [\varphi_a(\omega)]^l \exp(i\omega x)\, d\omega$, $l = 1, 2, \ldots$, such that $\operatorname{supp} \mathrm{ch}_{a,l}(x) = \left[\dfrac{-l}{(a-1)}, \dfrac{l}{(a-1)}\right]$ and $\int_{-l(a-1)^{-1}}^{l(a-1)^{-1}} \mathrm{ch}_{a,l}(x) dx = 1$. An important property of this function lies in the fact that its FT for even subscript $\int_{-\infty}^{\infty} \mathrm{ch}_{a,2l}(x) \exp(-i\omega x)\, dx = [\varphi_a(\omega)]^{2l}$ is nonnegative and no greater than unity. Feasible WFs are constructed with the aid of an expression in frequency domain $\Psi_r(\omega) = 1 - (1 - \varphi_a(\omega))^{r/2}$, $r = 2, 4, \ldots$, which is also positive and no greater than unity. Then the feasible WF is calculated as

$$K_{a,r}(x) = \frac{1}{2\pi}\int_{-\infty}^{\infty} \left\{1 - \left(1 - \varphi_a^2(\omega)\right)^{r/2}\right\} \exp(i\omega x)\, d\omega, \quad r = 2, 4, \ldots. \tag{18}$$

For several values of r, we obtain $K_{a,2}(x) = \mathrm{ch}_{a,1}(x)$, $K_{a,4}(x) = 2\,\mathrm{ch}_{a,1}(x) - \mathrm{ch}_{a,2}(x)$, and $K_{a,6}(x) = 3\,\mathrm{ch}_{a,1}(x) - 3\,\mathrm{ch}_{a,2}(x) + \mathrm{ch}_{a,3}(x)$. Figure 3 presents WFs $K_{a,r}(x)$ and their derivatives.

Estimation of quantity $f'(x)$ is written as

$$Df_n(x) = \frac{1}{nm^2}\sum_{j=1}^{n} N\left(\frac{X_j - x}{m}\right), \tag{19}$$

where $m = m(n)$ is the decreasing sequence of positive integers, $N(x)$ is the even function $\left(\int_{-\infty}^{\infty} N(x) dx = 1\right)$, and $N(x) \in L_2$. Using $N_r(x) = -K'_{r-1}(x)$, $r = 3, 5, \ldots$, we obtain feasible r-order WFs.

For the second derivative of the PDF, we have

$$D^2 f_n(x) = \frac{1}{nm^3}\sum_{j=1}^{n} M\left(\frac{X_j - x}{m}\right), \tag{20}$$

where $m = m(n)$ is the decreasing sequence of positive integers, $M(x)$ is the even function $\left(\int_{-\infty}^{\infty} M(x) dx = 1\right)$, and $M(x) \in L_2$. Using $M_r(x) = -K''_{r-2}(x)$, $r = 4, 6, \ldots$, we obtain feasible r-order WFs.

We consider *physical characteristics of the feasible WFs*. In the study of spectral kernels, we use the following modified physical characteristics [1]: width of the spectral density function (SDF) at a level of –3 dB γ_3, relative width of the SDF at a level of –6 dB γ_4/γ_3, HSLL (dB) γ_9, L_2 norm of WF P, uncertainty constant Δ, support "supp", and effective support $\mathrm{supp}_E = \{x \,|\, \|f(x)\|_{L_2} = 0.999P\}$. Table 8 presents the physical characteristics of WF $K_{a,r}(x)$ for several a and r.

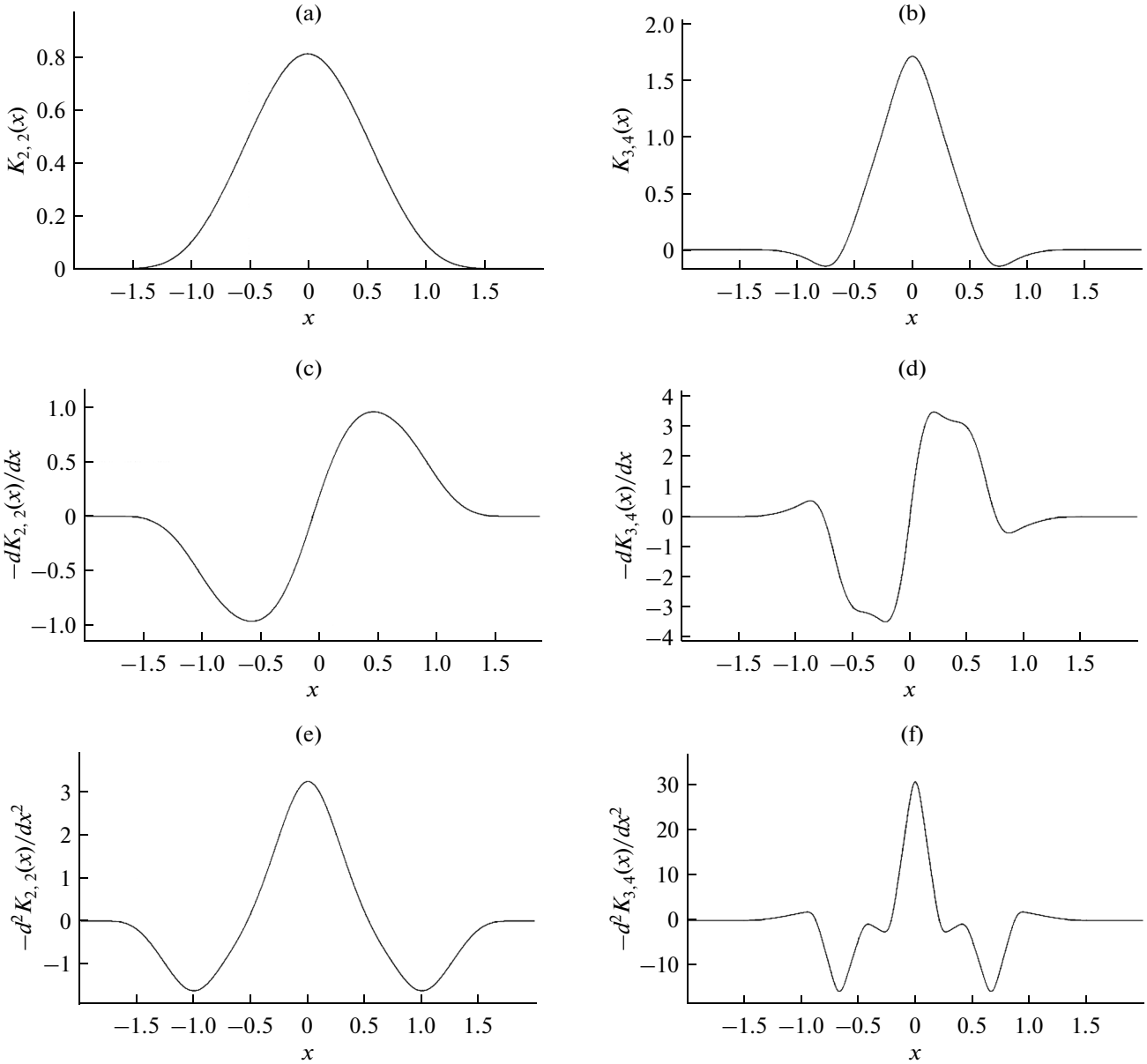

Fig. 3. (a) and (b) WFs $K_{a,r}(x)$ and their (c) and (d) first and (e) and (f) second derivatives for (a), (c), and (e) $a = 2$ and $r = 2$ and (b), (d), and (f) $a = 3$ and $r = 4$.

2.3. Numerical Experiment

By way of example, we consider estimation of PDF [28–36] of random series X_n with the normal distribution $f(x) = \frac{1}{\sqrt{2\pi\sigma^2}}\exp\left(-\frac{(x-\mu)^2}{2\sigma^2}\right)$, where the mean value is $\mu = 0.25$ and the RMS deviation is $\sigma = 0.5$ (Fig. 4a). Figures 4b–4d show the results of estimation of PDF $f(x)$ and the first two derivatives for $a = 2$, $r = 2$, and $n = 2500$.

We compare the characteristics of distributions that are calculated using the series and the corresponding estimations. Figures 5a and 5b present quantities $(\mu^* - \mu_n)$ and $(\sigma^* - \sigma_n)$, where

$$\mu^* = \frac{1}{\|f(x)\|^2}\int_{-\infty}^{\infty} x|f_n(x)|^2\,dx,$$

$$\sigma^* = \frac{1}{\|f_n(x)\|}\left(\int_{-\infty}^{\infty}(x-\mu^*)^2|f_n(x)|^2\,dx\right)^{1/2},$$

$$\mu_n = \frac{1}{n}\sum_{k=1}^{n}X_k,\ \sigma_n = \sqrt{\frac{1}{n}\sum_{k=1}^{n}(X_k-\mu_n)^2}.$$

Table 8. Physical characteristics of WFs $K_{a,r}(x)$ for several a and r

r	a	γ_3	γ_4/γ_3	γ_9	P	Δ	supp	supp_E
2	2	1.720	1.391	−46.59	0.945	0.502	4	2.029
	3	2.693	1.444	−34.03	0.735	0.508	2	1.233
	4	3.815	1.412	−30.49	0.622	0.513	4/3	0.898
	5	4.787	1.375	−28.99	0.549	0.518	1	0.708
	6	5.610	1.467	−28.21	0.496	0.522	4/5	0.587
	7	6.732	1.400	−27.76	0.456	0.525	2/3	0.501
4	2	2.581	1.232	−40.59	0.883	0.544	8	2.669
	3	4.114	1.236	−28.09	0.682	0.560	4	1.662
	4	5.610	1.240	−24.60	0.573	0.574	8/3	1.218
	5	7.181	1.229	−23.12	0.503	0.585	2	0.964
	6	8.602	1.239	−22.36	0.454	0.593	8/5	0.796
	7	10.098	1.222	−21.91	0.416	0.599	4/3	0.682
6	2	3.017	1.182	−37.08	0.852	0.588	12	2.669
	3	4.837	1.186	−24.66	0.654	0.614	6	1.674
	4	6.583	1.182	−21.21	0.547	0.638	4	1.225
	5	8.378	1.167	−19.76	0.478	0.656	3	0.972
	6	10.098	1.173	−19.01	0.429	0.670	12/5	0.805
	7	11.819	1.165	−18.57	0.393	0.680	2	0.687

It is seen that an increase in the WF order leads to a more smooth PDF and a decrease in the order results in a more accurate calculation of the mean value. Figures 5c and 5d illustrate variations in $(\sigma^* - \sigma_n)$ versus parameters a and r. Quantity σ^* is more accurately calculated when parameters a and r increase. To analyze the estimations, we calculate moments of PDF $m_k = \int_{-\infty}^{\infty} (x - \mu^*)^k f_n(x)\,dx$, asymmetry $A = m_3/\sigma^3$, and excess $E = m_4/\sigma^4 - 3$. Table 9 presents the results.

Thus, the AF theory is used to develop new WF structures with compact support. Feasible nonparametric estimations of probability density and its first and second derivatives are constructed for a random series. The parameters of function (2) make it possible to extend applicability of the proposed estimations and employ them in the analysis of various physical processes. The physical analysis proves the efficiency of the proposed nonparametric estimations of PDF.

3. AFs AND SYSTEMS OF PHASE LOCKING WITH SAMPLES

Phase-locking systems (PLSs) [37–40] are widely used for generation of high-precision oscillations in frequency synthesizers, optimal detection and coherent processing of discrete and continuous signals, and parallel computations in multiprocessor (cluster) systems. Note that PLSs with sampling (pulsed PLSs) in which the information on error in the self-control loop is processed at discrete moments differ from continuous PLSs in which the error signal is a continuous function of time. In practice, such systems employ specific pulsed phase discriminators (PPDs). Widely spread PPDs are based on the sampling and storage schemes. Differential equations are often used as mathematical models of PLSs with sampling. A specific feature of such systems (phase difference of synchronized oscillations is corrected at discrete moments) is disregarded. Such an approach is possible only for certain parameters of the PLS. In particular, we may assume that a differential equation serves as a mathematical model for the PLS with sampling if a proportional-integration filter in the self-control circuit has a time constant that is significantly greater than the repetition period of the control pulses of a tunable oscillator. In general, such an assumption is incorrect. A difference equation serves as an exact mathematical model for the PLS with sampling.

Most methods for the study of the PLSs with sampling that employ difference equations are not based on rigorous procedures of the theory of discrete mapping [37–40] and may disregard several physical effects of PLSs. A detailed analysis of the dynamics of

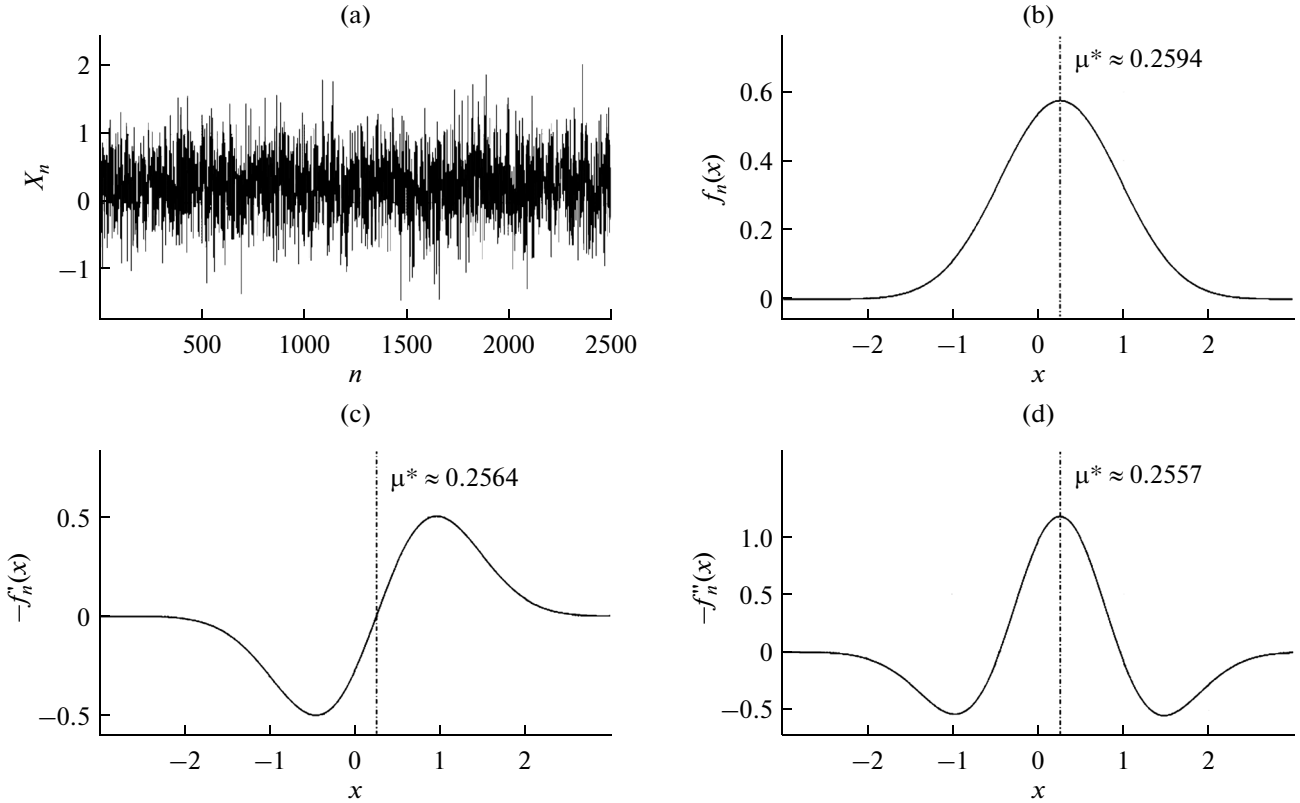

Fig. 4. (a) Random series X_n ($n = 2500$) and estimated (b) $f_n(x)$, (c) $Df_n(x)$, and (d) $D^2 f_n(x)$ for $a = 2$ and $r = 2$.

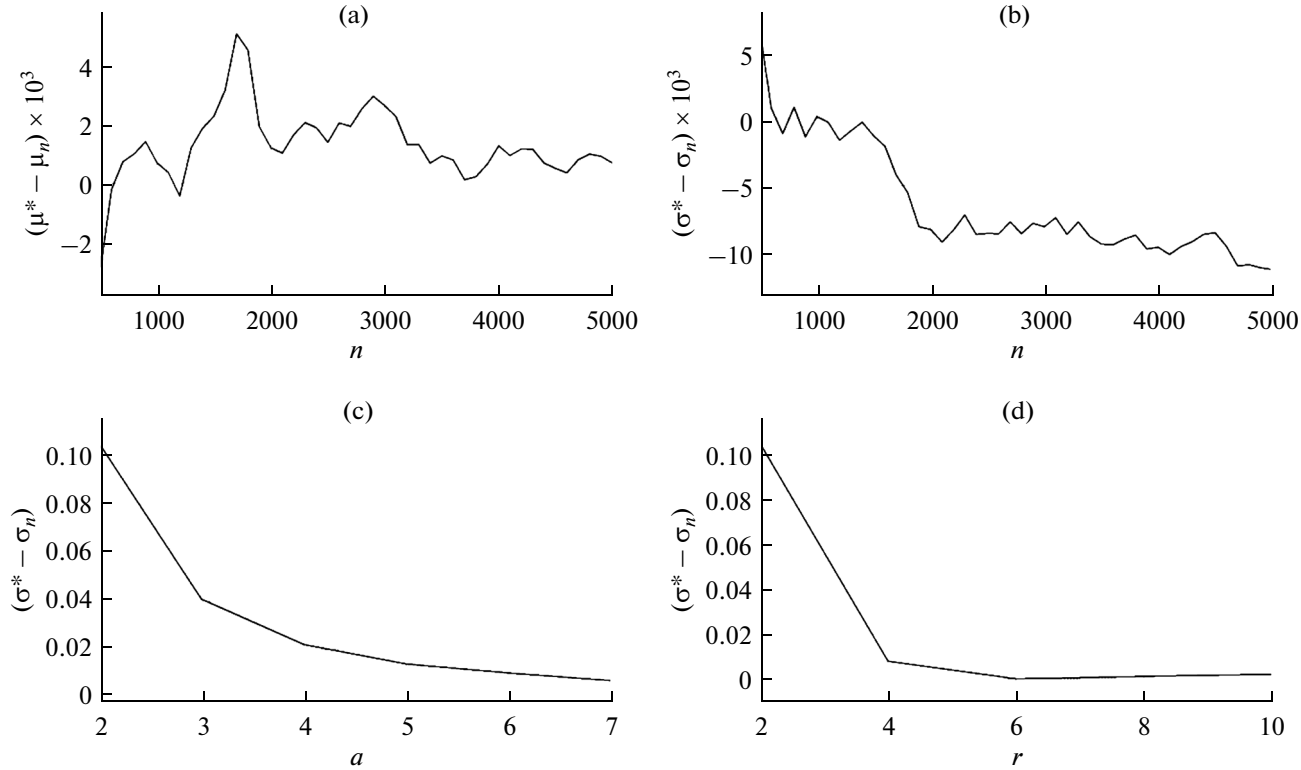

Fig. 5. Plots of (a) $(\mu^* - \mu_n)$ and (b) $(\sigma^* - \sigma_n)$ vs. n at $a = 2$ and $r = 2$ and $(\sigma^* - \sigma_n)$ vs. (c) a at $r = 2$ and (d) r at $a = 2$ ($n = 2500$).

Table 9. Characteristics of PDF estimations for random series X_n at $n = 2500$

r	a	μ^*	σ^*	$m_1 \times 10^3$	m_2	$m_3 \times 10^3$	m_4	$A \times 10^3$	$E \times 10^3$
2	2	0.524	1.103	–4.78	1.218	–32.41	4.437	–24.13	–6.68
	3	0.524	1.039	–5.49	1.079	–32.72	3.495	–29.20	3.94
	4	0.525	1.020	–5.77	1.040	–32.93	3.250	–31.06	6.24
	5	0.525	1.011	–5.96	1.023	–33.23	3.148	–32.11	7.18
4	2	0.525	1.006	–5.73	0.995	–32.06	2.684	–31.53	–375.35
	3	0.525	0.999	–5.94	0.995	–32.66	2.938	–32.75	–51.58
	4	0.525	0.999	–6.12	0.995	–33.22	2.968	–33.35	–16.61
	5	0.525	0.999	–6.32	0.995	–33.81	2.975	–33.95	–7.30
6	2	0.525	0.998	–5.95	0.995	–32.71	2.980	–32.94	8.01
	3	0.525	0.999	–5.99	0.995	–32.83	2.980	–32.94	–6.56
	4	0.525	0.999	–6.24	0.995	–33.57	2.980	–33.69	–6.15
	5	0.525	0.999	–6.47	0.995	–34.24	2.980	–34.37	–5.11
8	2	0.525	0.999	–5.99	0.995	–32.82	2.980	–32.94	–5.83
	3	0.525	0.999	–6.03	0.995	–32.94	2.980	–33.01	–11.20
	4	0.525	0.999	–6.32	0.995	–33.82	2.979	–33.92	–8.45
	5	0.525	0.999	–6.56	0.995	–34.52	2.980	–34.63	–7.30

PLSs with sampling must be based on the methods of the theory of discrete mapping. An important intrinsic feature of the PLSs with sampling is the presence of multiple zones of synchronous regimes with fractional multiplicity of frequency. Limited applications of such a feature for the frequency synthesis are due to the fact that spectrum of generated oscillations in the physical zones of synchronism of fractional multiplicities is contaminated with undesired components owing to the nonuniform distribution of the samples of input signal on the time axis. In the vicinity of the boundaries of the physical zones of synchronism, the spectrum of generated signals is destroyed. One of the methods for elimination of spectral contamination is based on the application of input signals with different waveforms. The AF theory is widely used at present in the problems of ultrabroadband radars and digital processing of signals and images [1–15]. However, the analysis of the generation of signals based on AFs is missing in literature. Thus, we concentrate on such a problem related to the generation of oscillations with pure spectra in the PLSs with sampling.

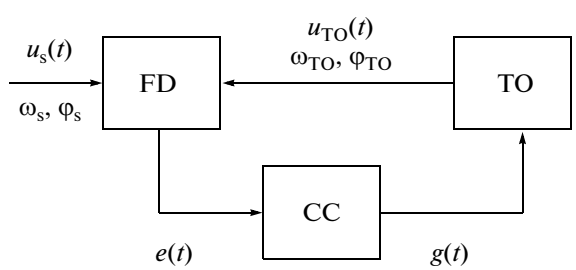

Fig. 6. Block diagram of PLS.

3.1. Basic Principles of the PLS Theory, Structural Scheme, Differential Equations, and Synchronization Zone

The concept of synchronization with the aid of PLSs is based on the measurement of the current phase mismatch of oscillations of a tunable oscillator (TO) and the generator of a reference oscillation with the subsequent use of the error signal for the correction of the frequency and phase of the TO. Figure 6 presents the structural scheme of the simplest continuous PLS. The basic principles are as follows. In phase discriminator (PD), current phase of reference signal $\varphi_s(t)$ is compared with TO oscillations phase $\varphi_{TO}(t)$ and error signal $e(t)$ is generated. Such a signal is delivered to the TO via a control circuit (CC). Control voltage $g(t)$ is transformed into correcting mismatch that is added to the TO frequency to provide a decrease in the original phase difference $\varphi(t) = \varphi_s(t) - \varphi_{TO}(t)$ of the TO oscillations and reference signal.

The differential equation that serves as a mathematical model of the PLS under study is generally represented as

$$\frac{p\varphi}{\Omega} + K(p)F(\varphi) = \gamma. \quad (21)$$

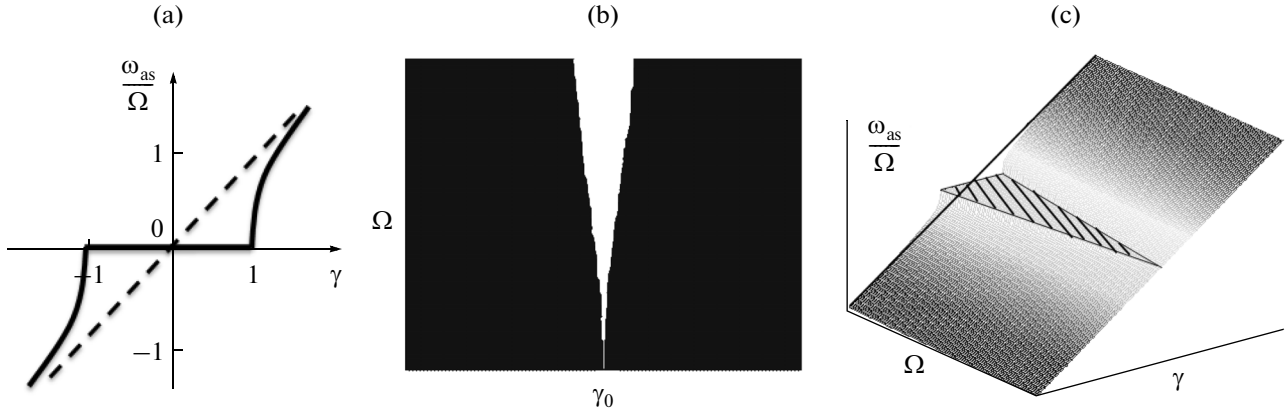

Fig. 7. (a) Plot of normalized frequency of asynchronous oscillations ω_{as}/Ω vs. mismatch, (b) physical zone of synchronism (Arnold tongue) on the (Ω, γ) plane, and (c) 3D map of the PLS zone of synchronism in the absence of filter.

Here, $\Omega = SE$ is the maximum correcting mismatch that is generated in the system, S is the slope of the control characteristics of the TO frequency control, E is the amplitude of the input signal, $\gamma = \frac{\omega_{TO} - p\varphi_s}{\Omega}$ is the dimensionless mismatch of TO frequency ω_{TO} relative to current frequency $\omega_s = p\varphi_s$ of the reference oscillation, $K(p)$ is the operator gain of the filter in the CC, $p \equiv d/dt$ is the symbolic representation of the differentiation operator, $F(\varphi)$ is the discrimination characteristics of the PD ($F(\varphi) = \sin\varphi$). Parameter $\Omega = SE$ is also known as the synchronization band of the PLS, since the synchronous regime in the PLS is reached at $\left|\omega_{TO} - \omega_s^0\right| \le \Omega$ (or $\gamma \le 1$). In the asynchronous regime that is observed outside the synchronization band, the current phase difference of the oscillations infinitely increases. Figure 7a presents the dependence of the normalized frequency of asynchronous oscillations ω_{as}/Ω on mismatch γ. It is seen that the frequency of asynchronous oscillations is zero inside synchronization band Ω (at $\gamma \le 1$) and the frequency of asynchronous oscillations increases as $\omega_{as}/\Omega = \sqrt{\gamma^2 - 1}$ outside the synchronization band. Figure 7b shows the synchronization band $\gamma_s = \frac{\omega_{synchr} - \omega_s}{\Omega}$ (Arnold tongue) on the plane of control parameters Ω and γ. Figure 7c presents the 3D map of the synchronous and asynchronous regimes of the PLS in the absence of filter.

Below, we obtain mathematical models of the PLSs with sampling for two scenarios (control of the TO frequency and period, respectively). We will also show that the difference equation for the PLS with sampling under control of the TO oscillation period can be derived using the discretization of differential equation (21) for the continuous PLS with a discretization step of unity.

We analyze *the working principles of the PLS with sampling*. Figure 8a shows the corresponding scheme. We consider harmonic input signal $u_s(t)$ (e.g., the signal of a reference oscillator) with amplitude U_0 and frequency $\omega_s = 2\pi/T_s$, where T_s is the period of the signal with initial phase θ_0. The following general expression is valid for $u_s(t)$:

$$u_s(t) = U_0 \sin[\omega_s t + \theta_0] = U_0 \sin[\varphi_s(t)]. \quad (22)$$

In the PPD scheme, samples u_k of input signal $u_s(t)$ are measured at moments t_k that correspond to the leading edge of the oscillations of the pulse shaper (PS) (Fig. 8b). In the absence of the filter in the PLS, the control voltage g_k that is fed to the TO input is e_k. Moment t_{k+1} of the next sample is controlled using variations in the TO oscillation period and frequency. We consider both variants [37–40].

(i) *Control of the TO oscillation period*. In this case, voltage g_k linearly controls interval $T_{k+1} = t_{k+1} - t_k$ between the sampling moments (i.e., TO oscillation period):

$$T_{k+1} = t_{k+1} - t_k = T_f - S_T g_k, \quad (23)$$

where T_f is the period of the free TO oscillations at $g_k \equiv 0$ and S_T is the slope of the modulation characteristic of the unit that controls the TO period. With allowance for expression (22), we obtain the following dependence $t_{k+1} = f(t_k)$ using formula (23):

$$t_{k+1} = t_k + T_f - T_m \sin[\omega_s t_k + \theta_0], \quad (24)$$

where $T_m = S_T U_0$ is the maximum deviation of the TO oscillation period. To analyze phase samples $\varphi = \omega_s t + \theta_0$, we multiply expression (24) by ω_s and add initial phase θ_0. Using the maximum phase deviation $K = \omega_s T_m$, we have

$$\varphi_{k+1} = \varphi_k + 2\pi B - K \sin\varphi_k, \quad (25)$$

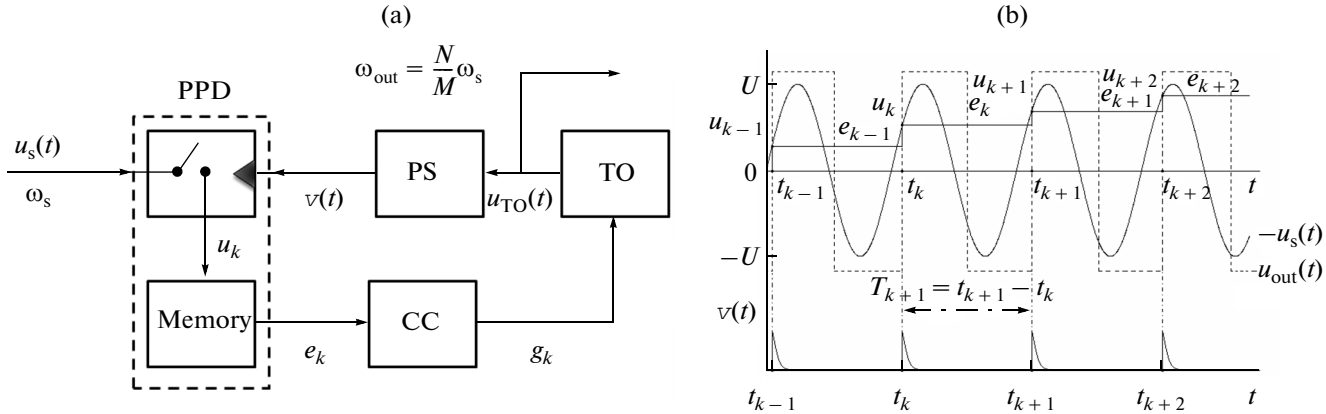

Fig. 8. (a) Block diagram of sampling PLS and (b) sampling of the input sine-shaped signal.

where $B = T_f/T_s = \omega_s/\omega_f$ is the initial frequency mismatch of the signal and free oscillations of TO. We divide difference equation (25) by 2π and employ coordinate $x_k = \varphi_k/2\pi$:

$$x_{k+1} = x_k + B - (K/2\pi)\sin(2\pi x_k). \quad (26)$$

Difference equation (26) serves as the mathematical model of the sampling PLS under control of the TO oscillation period.

(ii) *Control of the TO oscillation frequency.* To obtain the difference equation for the frequency-control of the TO oscillations, we consider voltage g_k that linearly controls the TO oscillation frequency:

$$\omega_{k+1} = \frac{2\pi}{T_{k+1}} = \frac{2\pi}{t_{k+1} - t_k} = \omega_f - S_\omega g_k. \quad (27)$$

Here, ω_f is the free-oscillation frequency at $g_k \equiv 0$ and S_ω is the slope of the modulation characteristic of the unit that controls the TO oscillation frequency. Let $\omega_m = S_\omega U$ be the maximum correcting mismatch that is corrected by the control unit. In expression (27), we substitute quantity e_k for voltage g_k. Thus, we derive an expression that is similar to expression (24):

$$t_{k+1} = t_k + \frac{2\pi}{\omega_f - \omega_m \sin[\omega_s t_k + \theta_0]}. \quad (28)$$

First, we consider the difference equation for current phase $\varphi_k = \omega_s t_k + \theta_0$. Using coefficients $\gamma = 2\pi\omega_s/\omega_f$ and $\Omega_\omega = \omega_m/\omega_f$, we obtain

$$\varphi_{k+1} = \varphi_k + \frac{\gamma}{1 - \Omega_\omega \sin\varphi_k}. \quad (29)$$

To finalize the construction of the mathematical model of the sampling PLS under control of the TO oscillation frequency [37], we use normalized phase $x_k = \varphi_k/2\pi$. Thus, we have

$$x_{k+1} = x_k + \frac{B_\omega}{1 - K_\omega \sin(2\pi x_k)}. \quad (30)$$

Expressions (26) and (30) represent mathematical models of the sampling PLS (two-parameter difference equations or discrete mappings) for the systems with the period and frequency control, respectively. Mapping (26) can be obtained with the aid of the discretization of the differential equation of the continuous PLS. Using discretization step h, we change continuous time t in differential equation (21) by discrete time $t_n = nh$ ($n = 0, 1, 2, ...$). In this case, observations in continuous time $\varphi(t)$ are changed by a time series of discrete observations $\varphi_n = \varphi(t_n)$ at equidistant points of the discrete time scale. The discretization of the derivatives of a measurable quantity is performed using the Euler method in which the first derivative $d\varphi(t)/dt$ is changed by the first difference $(\varphi_{n+1} - \varphi_n)/h$. For the PLS in the absence of the filter, we have $K(p) \equiv 1$. In this case, differential equation (14) in continuous time is changed by its model in discrete time n, so that $\varphi_{n+1} = \varphi_n + h\Omega(\gamma - \sin[\varphi_n])$ for the sine-shaped characteristic of the PD.

Using dimensionless phase $x_n = \varphi_n/2\pi$, we transform the last expression dividing both sides by 2π:

$$x_{n+1} = x_n + B(h) - K(h)\sin[2\pi x_n]. \quad (31)$$

Here, we use coefficient $B(h) = h\Omega\gamma/2\pi$ that characterizes the frequency mismatch of the TO free oscillations and reference signal and control coefficient $K(h) = h\Omega/2\pi$. Both coefficients depend on discretization step h. Figure 9 shows the functional scheme of difference equation (31). Here, we use the following initial data: dimensional mismatch γ^0, discretization step h, and initial phase difference φ_0. Current sample of the phase difference φ_n is the output coordinate. Mapping (31) coincides with mapping (25) but control parameters K and B depend on discretization step h. Below, we study mappings (26) and (30) and consider the dynamics of the sampling PLS. For simplicity, we consider the period-control of the TO oscillations.

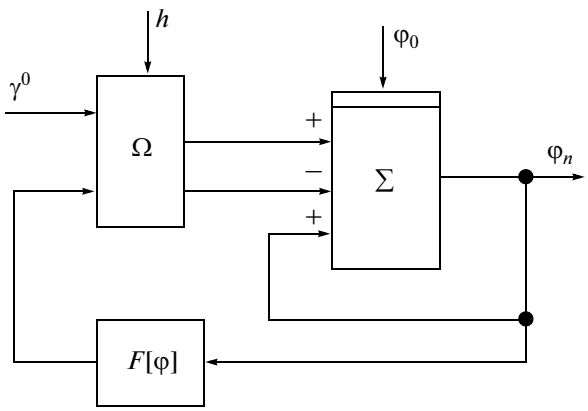

Fig. 9. Block diagram of PLS with discretization.

Analysis of dynamic processes in a sampling PLS. We consider methods to study the dynamics of mappings (26) and (30). Discrete mappings (difference equations) are considered on a cylindrical surface in accordance with the theory of continuous phase-locking systems [37–40]. Such a representation of the discrete mapping is convenient, since it allows the graphical representation of the dynamic process using the Lamerey–Königs diagrams. Figure 10 shows an illustration for mapping $x_{k+1} = f(x_k)$. The method is used to construct time processes x_k versus k (Fig. 10b). We study the output oscillations of the sampling PLS, so that Figs. 11a and 11c show the Lamerey–Königs diagrams and Figs. 11b and 11d show the time realizations of the original signal and samples.

Starting the analysis of the dynamics of mapping (26), note that difference equation (26) is similar to the mapping of the following circle:

$$x_{k+1} = x_k + B - (K/2\pi)\sin[2\pi x_k], \quad \mathrm{mod}(1). \qquad (32)$$

Substituting mapping (32) for mapping (26), we may obtain errors in the working PLS. In the fractional multiple regime, we consider the difference of the mappings. Let the frequency mismatch of the signal and TO be $B \approx 0.5$, so that two samples correspond to one period of the input signal (Fig. 11a). When $B \approx 1.5$, two samples correspond to three periods of the input signal (Fig. 11b).

We consider mapping (32) for parameters $B = 0.5$ and 1.5.

(i) For $B = 0.5$, we have

$$x_{k+1} = x_k + 0.5 - (K/2\pi)\sin[2\pi x_k], \quad \mathrm{mod}(1),$$

(ii) For $B = 1.5$, we obtain

$$x_{k+1} = x_k + 1.5 - (K/2\pi)\sin[2\pi x_k]$$
$$= x_k + 0.5 - (K/2\pi)\sin[2\pi x_k], \quad \mathrm{mod}(1).$$

Thus, mapping (32) remains unchanged when the regime of frequency division is changed by the regime of frequency multiplication. The corresponding Lamerey–Königs diagrams are identical (Fig. 11). Such results may lead to significant errors in practice, so that mapping (26) must be employed. The above processes clearly differ in the corresponding diagrams (Fig. 12). Approximate equality is used to show the approximate frequency tuning of the signal and TO

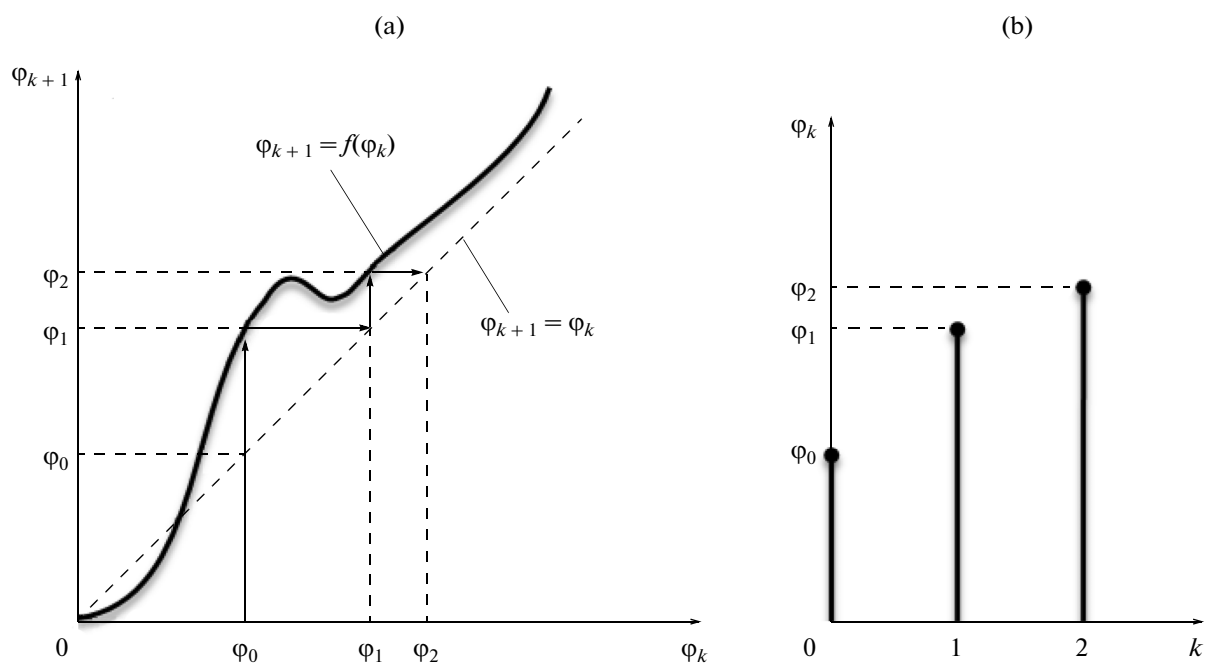

Fig. 10. (a) Lamerey–Königs diagram and (b) time process.

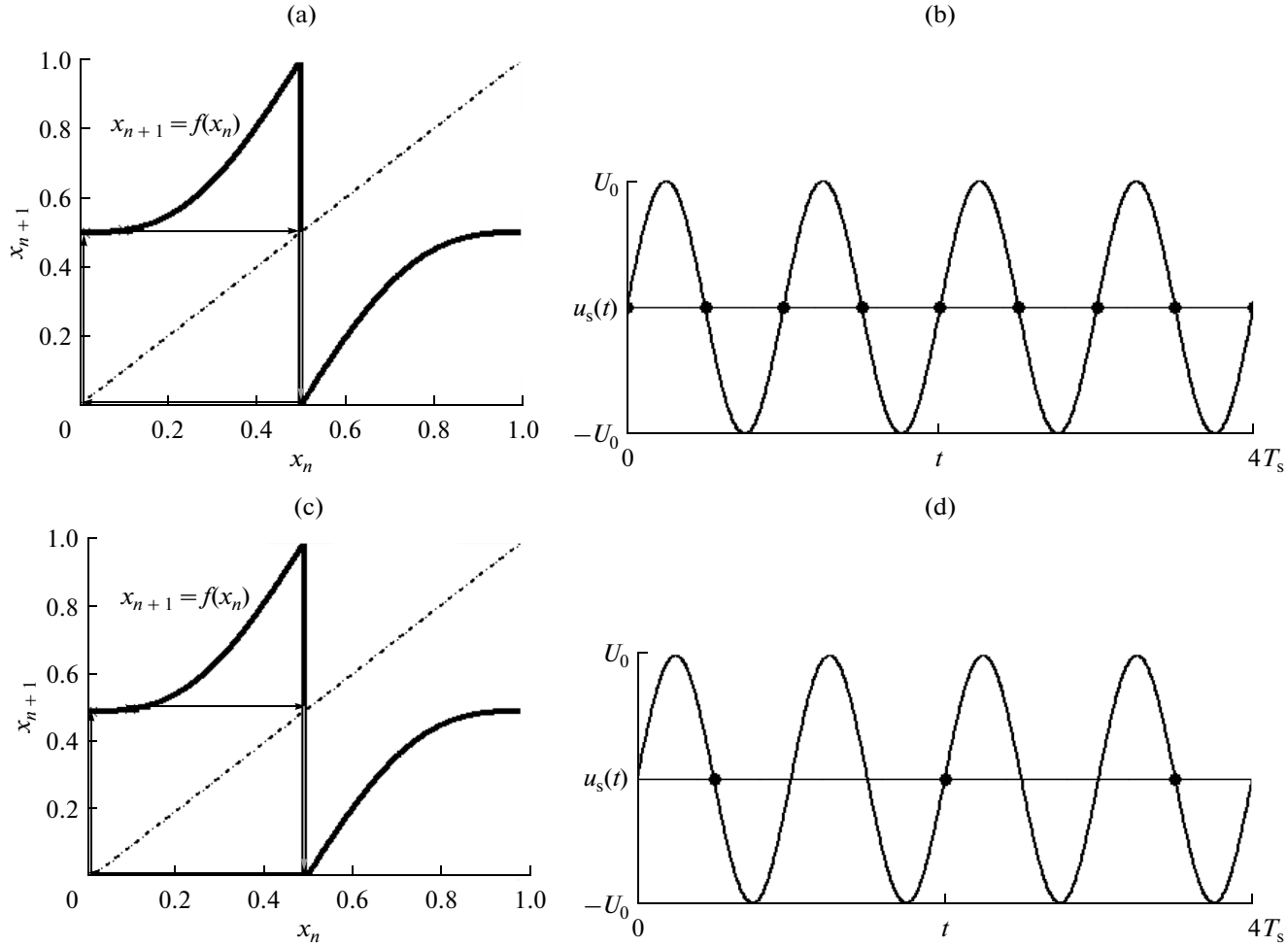

Fig. 11. (a) and (c) Lamerey–Königs diagram and (b) and (d) sample signals in time for (a) and (b) $K = 1$ and $B = 0.5$ and (c) and (d) $K = 1$ and $B = 1.5$.

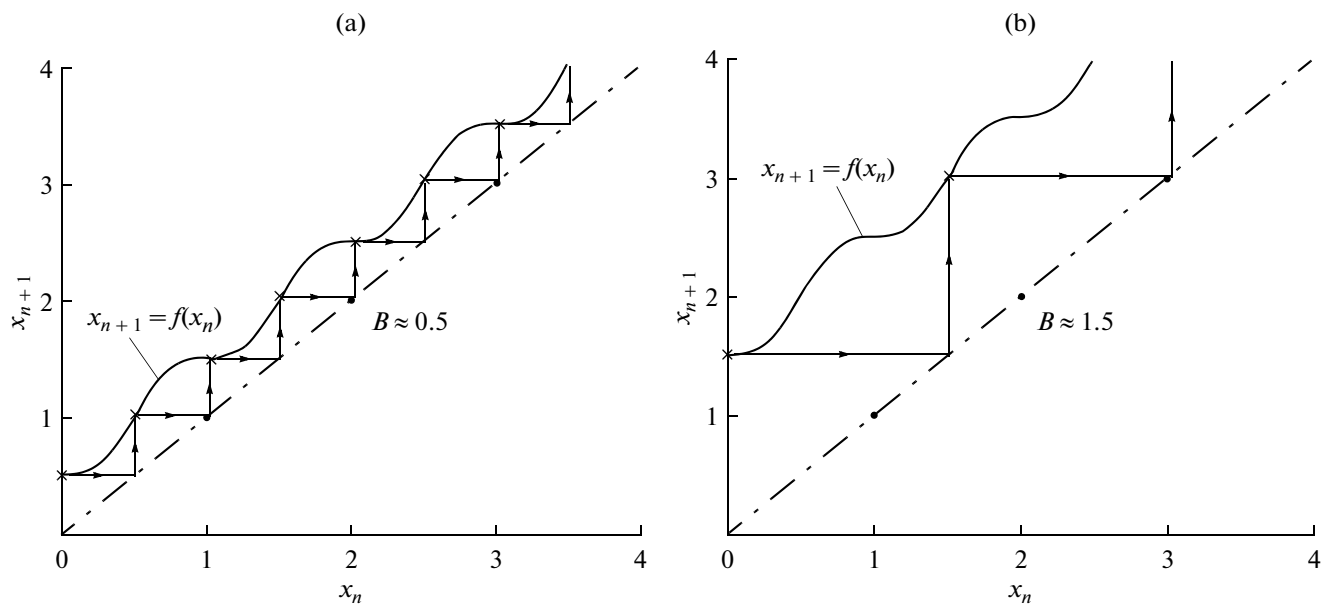

Fig. 12. Lamerey–Königs diagrams for the difference equation of sampling PLS for $B \approx$ (a) 0.5 and (b) 1.5.

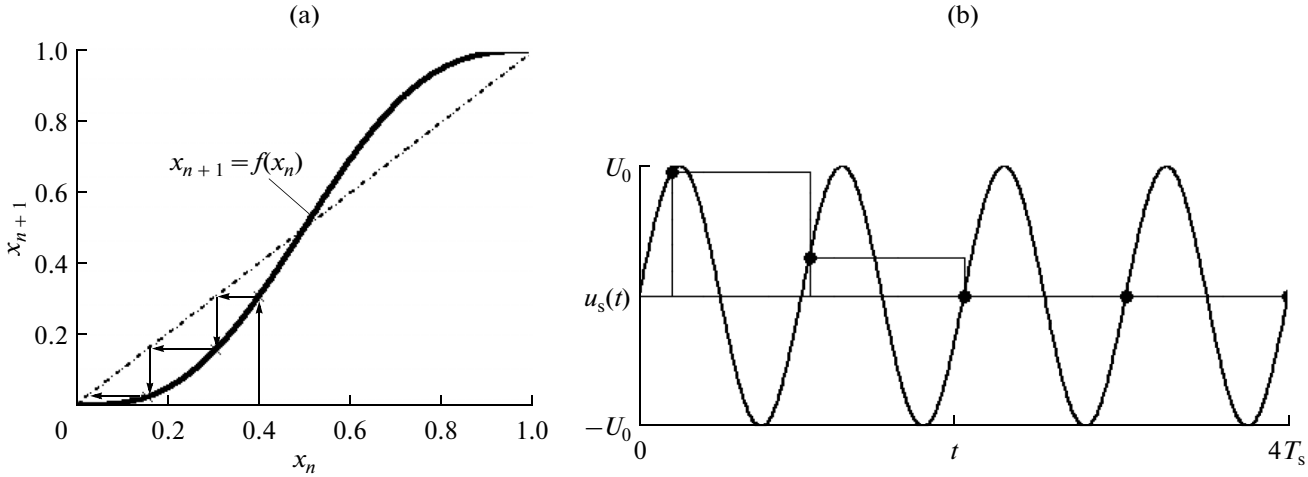

Fig. 13. (a) Lamerey–Königs diagram and (b) time process of mapping (6) for $K = 1$, $B = 1$, and $x_0 = 0.4$.

free oscillations. However, such an approach is cumbersome. The above errors do not emerge when $B < 1$. Thus, we consider such a scenario and employ mapping (32) for simplicity.

First, we consider the exact frequency tuning of the TO to the signal frequency ($B = 1$) when one sample corresponds to one period of the input signal. Figure 13 shows the corresponding diagram and the time process. Three fixed points ($\hat{x} = 0$, $\hat{x} = 0.5$ and $\hat{x} = 1$) exist in this case. Multiplicators must be used to study the stability.

Multiplicators μ of the above points (i.e., slopes of mapping function

$$f(x_k, B, K) = x_k + B - (K/2\pi)\sin(2\pi x_k)$$

are found from the following expression:

$$\mu = \frac{\partial f(\hat{x}, B, K)}{\partial \hat{\phi}} = 1 - K\cos(2\pi\hat{x}). \quad (33)$$

It is seen that the multiplicator is 0 at two points ($\hat{x} = 0$ and $\hat{x} = 1$) and 2 at $\hat{x} = 0.5$, when $K = 1$. Thus, the last point is unstable. For $B = 0.5$, we may obtain the $2T$ cycle. In this case, we must study fixed points of double mapping $f(f(x, B, K), B, K)$. Figure 14 presents the Lamerey–Königs diagram for the mapping of circle at $B = 0.5$ when the TO frequency is equal to the doubled frequency of the input signal. A similar procedure can be used to analyze alternative scenarios. Consider the dynamic regimes for the sampling PLSs.

Map of dynamic regimes of a sampling PLS. When parameters K and B are varied in wide ranges, we may obtain various types of motion. Figures 15a–15c present the simplest motions ($2T$-, $3T$-, and $5T$-cycles). Similar scenarios are obtained for mapping (30).

For mappings (26) and (30), we may divide plane of parameters (K, B), and (K_ω, B_ω) [37] into domains with different types of motion. Such an approach is widely used in the theory of nonlinear dynamic systems, since it yields clear 2D maps needed for the development of recommendations for tuning of the sampling PLSs. In this case, it is expedient to use rotation number, which characterizes mean variation in the phase of the original signal per one iteration (sample):

$$W = \lim_{k\to\infty} \frac{x_k - x_0}{k}. \quad (34)$$

With allowance for a nonlinear function that controls the waveform of the input signal in the right-hand sides of mappings (26) and (30), we divide the plane of parameters (K, B) and (K_ω, B_ω) [37] into domains with different rotation numbers. Figure 16a presents the zones of synchronism (Arnold tongues) for rotation numbers of 1/3, 1/2, and 2/3 for $K \in [0,1]$. Figure 16a shows that the 1/2 zone is symmetric in contrast to the zones with multiplicities of 1/3 and 2/3. Figures 16b

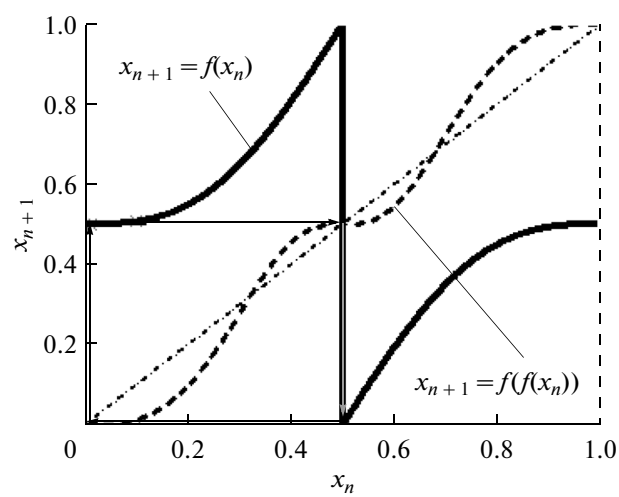

Fig. 14. (a) Lamerey–Königs diagram for $K = 1$ and $B = 0.5$.

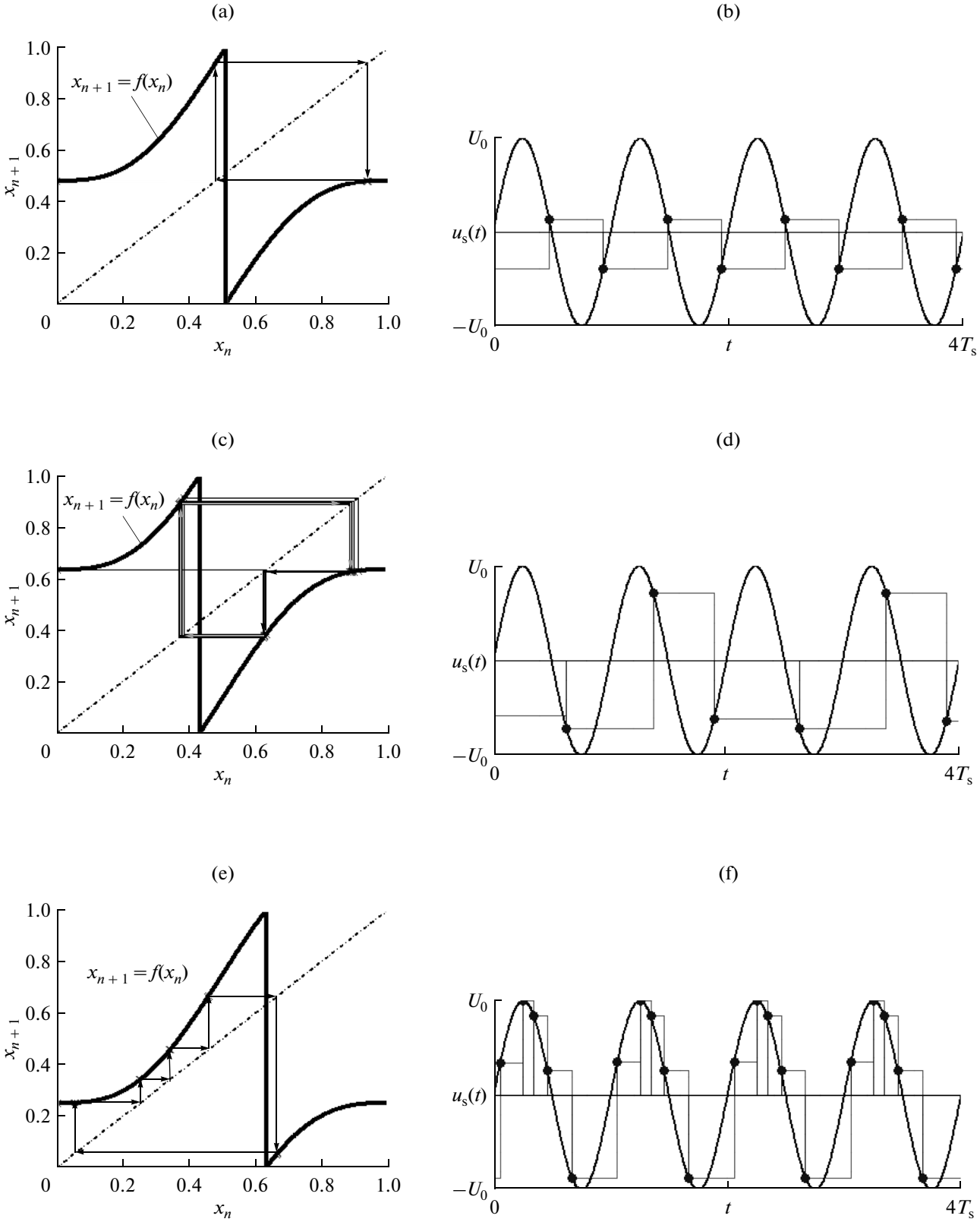

Fig. 15. Different types of motion: (a) $2T$ cycle ($B = 0.48$ and $K = 1$), (b) $3T$ cycle ($B = 0.6333$ and $K = 1$), and (c) $5T$ cycle ($B \approx 1/5$ and $K = 0.1$) and (b), (d), and (f) the corresponding samples of the input signal.

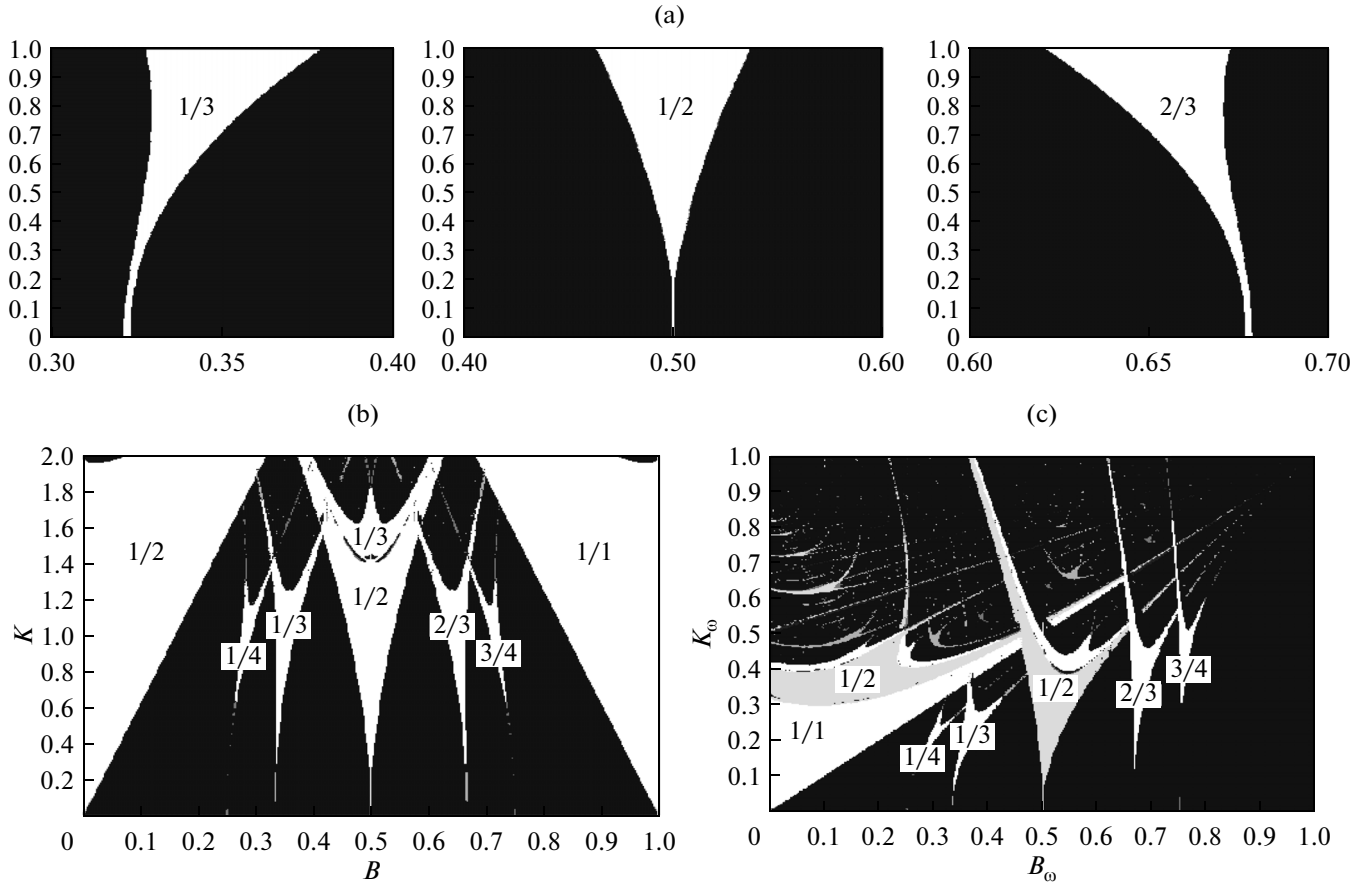

Fig. 16. (a) Physical zones of synchronism for multiplicities of 1/3, 1/2. and 2/3 on a large scale and expanded maps of dynamic regimes for (b) period- and (c) frequency-control of the TO oscillations.

and 16c present the expanded maps of dynamic regimes (synchronization zones) for the conventional and modified mappings of the circle for $K \in [0,2]$, $K_\omega \in [0,1]$, and $B, B_\omega \in [0,1]$.

The neighboring Arnold tongues can be overlapped at $K > 1$. In this case, the sampling PLSs exhibit chaotic oscillations.

The plot of the rotation number versus control parameter B at $K = 1$ (Fig. 17a) represents a self-similar structure (devil's staircase fractal). It consists of an infinite number of horizontal fragments (copies of the synchronism zones (Fig. 5a)) that are responsible for the synchronization at the fractional multiple frequencies. Figure 17b presents the 3D map of the dependence of the rotation number on control parameters B and K. It is similar to Fig. 7c and consists of an infinite number of zones of synchronous regimes with fractional multiplicity of frequency.

The sampling PLSs may exhibit multiple synchronous regimes with fractional multiplicity of frequency in the corresponding zones of synchronism (Arnold tongues). Such systems that make it possible to implement multiple zones of synchronism exhibit a significant disadvantage.

Prior to the analysis of the dynamics of mappings (26) and (30) in the corresponding synchronous physical zones, we study the effect of the waveform of the input signal on the map of the zones of synchronous regimes.

Periodic oscillations consisting of AFs serve as the reference input signals for sampling. We choose such an approach, since the application of oscillations consisting of shifted AFs provides the broadening of the zones of synchronous regimes for the PLSs with samples with fractional multiplicity of frequency (see below).

3.2. Elements of the AF Theory and the Methods for Formation of Periodic Signals

The results of [1, 5] show that AFs represent solutions to the FDEs

$$\frac{d^n y(x)}{dx^n} + a_1 \frac{d^{n-1} y(x)}{dx^{n-1}} + \ldots + a_{n-1} \frac{dy(x)}{dx} + a_n y(x) = \sum_{k=1}^{M} b_k y(ax - b_k), \quad (35)$$

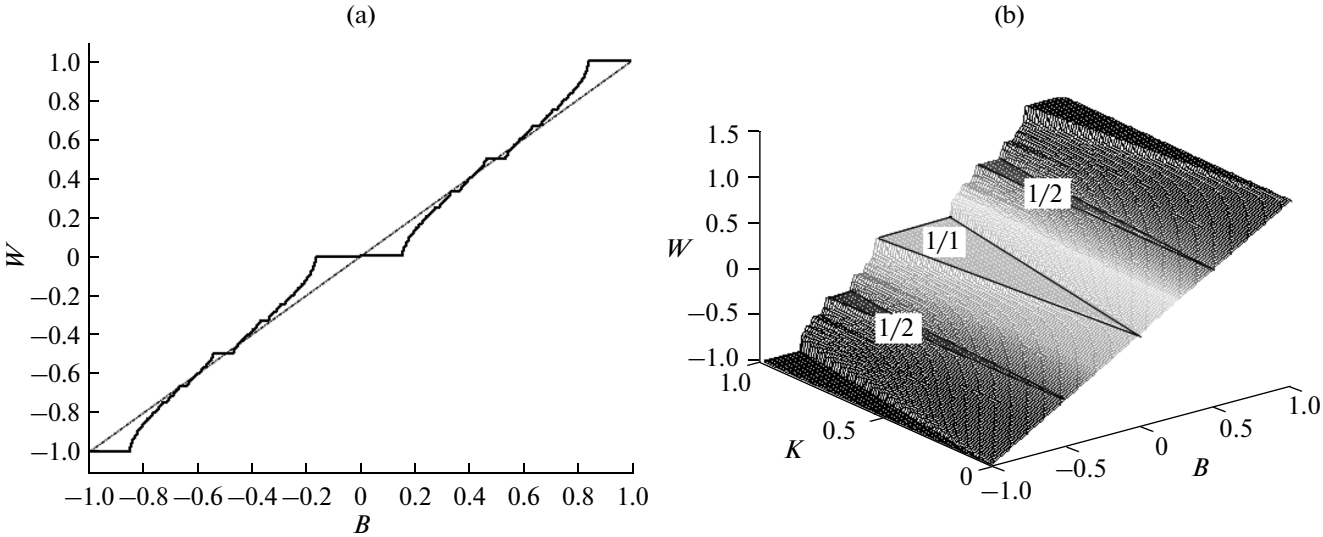

Fig. 17. (a) Plot of the rotation number on parameter B at $K = 1$ and (b) 3D map of rotation number W vs. parameters K and B.

where $|a| > 1$. When $b_k \equiv 0\ (k = 1,\ldots,M)$, expression (35) is transformed into a conventional differential equation. Using the shifts of the finite solution of Eq. (35), we may construct solutions to the homogeneous problem with the zero right-hand side. For example, the shifts of AF $y_k(x)$, that represent solutions to the FDE $\frac{dy(x)}{dx} - ky(x) = \alpha_1 y(2x+1) - \alpha_2 y(2x-1)$ can be used to construct the solution to homogeneous problem $\frac{dy(x)}{dx} - ky(x) = 0$:

$$\sum_{j=-\infty}^{\infty} c_j y_k(x-j) = C\exp(kx).$$

Such an approach makes it possible to solve complicated ODEs with variable coefficients that do not allow analytical solutions [5, 38]. We consider an operator method to solve Eq. (35) and assume that $d/dx \equiv p$. Then, the action of operator p on function $y(x)$ is equivalent to the differentiation $py(x) = \frac{dy(x)}{dx}$ and the n-th derivative of function $y(x)$ with respect to x is written as $p^n y(x) = \frac{d^n y(x)}{dx^n}$. Expression $y(ax - b_k)$ is symbolically represented as $y(ax - b_k) = y(a(x - b_k/a)) = \exp\left(-\frac{b_k}{a}p\right)y(ax)$. In the operator representation, Eq. (35) is represented as

$$\sum_{j=0}^{n} a_{n-j} p^j [y(x)] = \sum_{k=1}^{M} b_k \exp\left(-\frac{b_k}{a}p\right)[y(ax)]. \quad (36)$$

Here, $[y(x)]$ denotes the action of operator $A(p)$ on function $y(x)$. Expression (36) can be represented as a relationship of function $y(x)$ and contracted function $y(ax)$:

$$y(x) = K(p)[y(ax)], \quad (37)$$

where

$$K(p) = \frac{\sum_{k=1}^{M} b_k \exp\left(-\frac{b_k}{a}p\right)}{\sum_{j=0}^{n} a_{n-j} p^j}.$$

We assume that function $y(x)$ is a finite function and determine the corresponding analytical representation as the infinite action of operator $K(p)$ on δ function:

$$y(x) = \prod_{i=0}^{\infty} K\left(\frac{p}{a^i}\right)[\delta(x)]. \quad (38)$$

The above operator method makes it possible to derive analytical solutions to FDEs (35) with variable coefficients if $a_i = a_i(x)$. Expression (38) can be interpreted in the following way: finite AF $y(x)$ is a response of filter with transfer function $\prod_{i=0}^{\infty} K\left(\frac{p}{a^i}\right)$ to δ function (i.e., pulse response of the filter). Therefore, a filter with transfer function $\prod_{i=0}^{\infty} K\left(\frac{p}{a^i}\right)$ must be constructed for the formation of AF $y(x)$. Such a filter contains a cascade of inertial units $\left(\sum_{j=0}^{n} a_{n-j}\left(\frac{p}{a^i}\right)^j\right)^{-1}$, $i = 1, 2, \ldots$ and delay lines $\sum_{k=1}^{M} b_k \exp\left(-\frac{b_k}{a}\left(\frac{p}{a^i}\right)\right)$, $i = 1, 2, \ldots$. An alternative method can be used to construct a filter with operator transfer coefficient

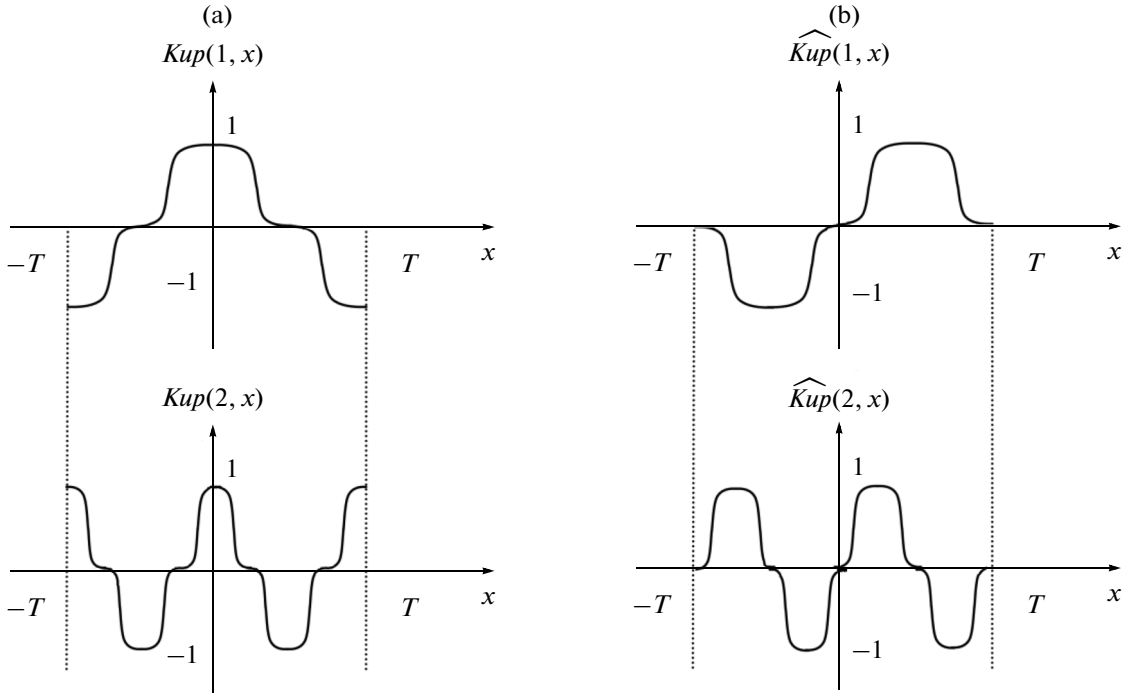

Fig. 18. (a) Even and (b) odd first basis functions that are constructed using shifted AFs $up(x)$.

$\Xi(p) = \prod_{i=0}^{\infty} K\left(\frac{p}{a^i}\right)$. To obtain frequency response (FR) $\Xi(j\omega)$ of the filter with operator transfer coefficient $\Xi(p)$, we must use $p = j\omega$. After such a substitution and calculation of $\Xi(j\omega)$, we can use conventional methods for the synthesis of filters based on the FRs using the Butterworth and Chebyshev methods. Function $y(x)$ that results from the solution of FDE (35) is a finite function. Note the importance of the construction of periodic signals using the shifts of such function. The problem has been formulated and solved in [37–40] for AF $up(x)$. Notation $Kup(x)$ and $\widehat{Kup}(x)$ was used for the orthogonal periodic even and odd systems of the Kravchenko functions, respectively. We consider the method for construction of such functions. AF $up(x)$ is a finite solution to the FDE

$$up'(x) = 2(up(2x+1) - up(2x-1)). \tag{39}$$

Operator $\Xi(p)$ for FDE (39) is written as

$$\Xi(p) = \prod_{i=1}^{\infty} \frac{\sinh\left(p/2^i\right)}{\left(p/2^i\right)}. \tag{40}$$

To obtain the FR of the filter with pulse response $up(x)$, it is suffice to assume that $p = j\omega$ in formula (40) and calculate the Fourier transform of expression (38). Using formula (40), we obtain

$$\Xi(j\omega) = \prod_{i=1}^{\infty} \frac{\sinh\left(j\omega/2^i\right)}{\left(j\omega/2^i\right)} = \prod_{i=1}^{\infty} \frac{\sin\left(\omega/2^i\right)}{\left(\omega/2^i\right)}. \tag{41}$$

Thus, function $up(x)$ can be calculated using its representation as inverse Fourier transform of function (41).

Even and odd systems of periodic functions on segment $[-T, T]$ are represented in the following way.

(i) For even functions we have

$$Kup(0,x) = 1,$$

$$Kup(1,x) = up\left(\frac{2}{T}x\right) - up\left(\frac{2}{T}(x-T)\right) - up\left(\frac{2}{T}(x+T)\right),$$

$$Kup(2,x) = up\left(\frac{4}{T}x\right) - up\left(\frac{4}{T}\left(x - \frac{T}{2}\right)\right)$$
$$- up\left(\frac{4}{T}\left(x + \frac{T}{2}\right)\right) + up\left(\frac{4}{T}(x-T)\right) + up\left(\frac{4}{T}(x+T)\right),$$

(ii) For odd functions we have

$$\widehat{Kup}(0,x) = 0,$$

$$\widehat{Kup}(1,x) = up\left(\frac{2}{T}\left(x - \frac{T}{2}\right)\right) - up\left(\frac{2}{T}\left(x + \frac{T}{2}\right)\right),$$

$$\widehat{Kup}(2,x) = up\left(\frac{4}{T}\left(x - \frac{T}{4}\right)\right) - up\left(\frac{4}{T}\left(x - \frac{3T}{4}\right)\right)$$
$$- up\left(\frac{4}{T}\left(x + \frac{T}{4}\right)\right) + up\left(\frac{4}{T}\left(x + \frac{3T}{4}\right)\right),$$

Figure 18 illustrates the formation of systems of even $Kup(1,x)$, $Kup(2,x)$ and odd $\widehat{Kup}(1,x)$, $\widehat{Kup}(2,x)$ Kravchenko functions.

A similar procedure for the construction of periodic oscillations using the joining of elementary pulses

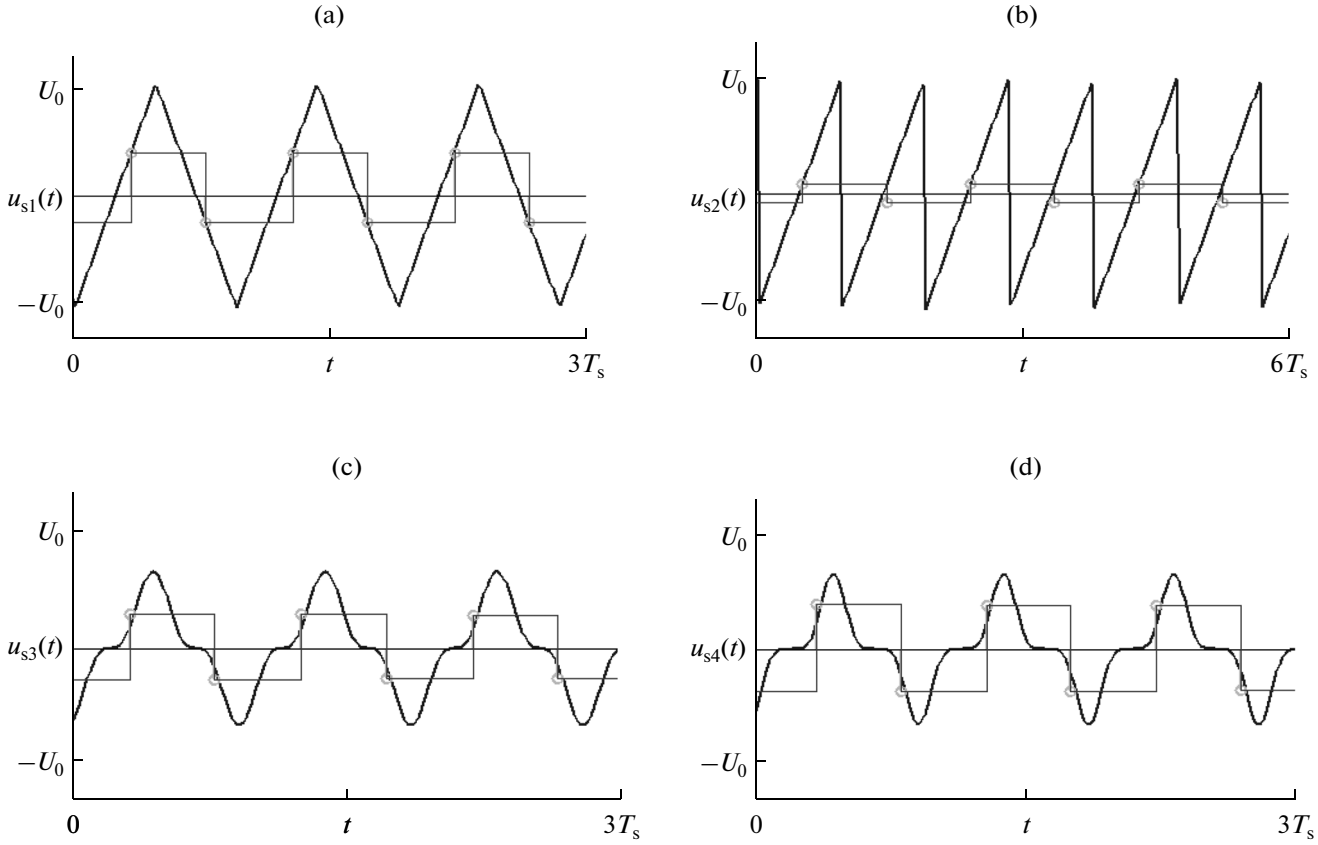

Fig. 19. Different waveforms $u_{c1\text{–}5}(t)$ corresponding to different nonlinearities $F_{1\text{–}5}[x]$ in (42).

can be used for arbitrary finite solutions of FDE (35). For example, AFs $fup_n(x)$ that represent solutions to FDE

$$fup_n'(x) = 2^{n-1}\sum_{k=0}^{n+2}\left(C_{n+1}^{k} - C_{n+1}^{k-1}\right) \times fup_n\left(2^{n-1}x - \frac{2(k-1)-n}{2^{n+2}}\right)$$

are determined as

$$fup_n(x) = \frac{1}{2\pi}\int_{-\infty}^{\infty}\operatorname{sinc}^n\left(\frac{\omega}{2}\right)\prod_{i=1}^{\infty}\operatorname{sinc}\left(\frac{\omega}{2^i}\right)\exp(i\omega x)\,d\omega.$$

The notation for such system is $Kfup_n$ and $\widehat{Kfup}_n(x)$ (similarly to $Kup(x)$ and $\widehat{Kup}(x)$). We consider modifications of the physical map of the PLS dynamic regimes using periodic signals Kup and $Kfup_n$.

3.3. Effect of the Waveform of the Input Signal on the Map of Zones of Synchronous Regimes of Sampling PLSs

An important feature of the sampling PLSs lies in the fact that the map of dynamic regimes (zones of synchronous and asynchronous regimes) substantially depends on the waveform of the input signal. Difference equation (26) is represented with allowance for arbitrary waveform. Then, we have

$$x_{k+1} = x_k + B - (K/2\pi)F[x_k]. \tag{42}$$

Here $F[x]$ is the 2π periodic function (in expression (26), we have $F[x] = \sin(2\pi x)$). We study the effect of the waveform of the input signal (function $F[x]$ in expression (42)) on the physical map of the zones of synchronous regimes. We use the following functions

$$F_1[x] = \arcsin\{\sin(2\pi x)\}, \tag{43}$$

$$F_2[x] = \arctan\{\tan(2\pi x)\}, \tag{44}$$

$$F_3[x] = Kfup_3(2\pi x), \tag{45}$$

$$F_4[x] = Kfup_5(2\pi x), \tag{46}$$

$$F_5[x] = Kup(2\pi x). \tag{47}$$

Figure 19 shows the oscillograms of the input signals and the error signals in the regime of frequency doubling that correspond to functions $F_{1\text{–}5}[x]$. Figures 20a–20e and 21a–21e present the plots of rotation numbers W versus parameters B and K for input signals (43)–(46). Figures 21a–21e show the physical maps of the zones of synchronous regimes (Arnold tongues) on the plane

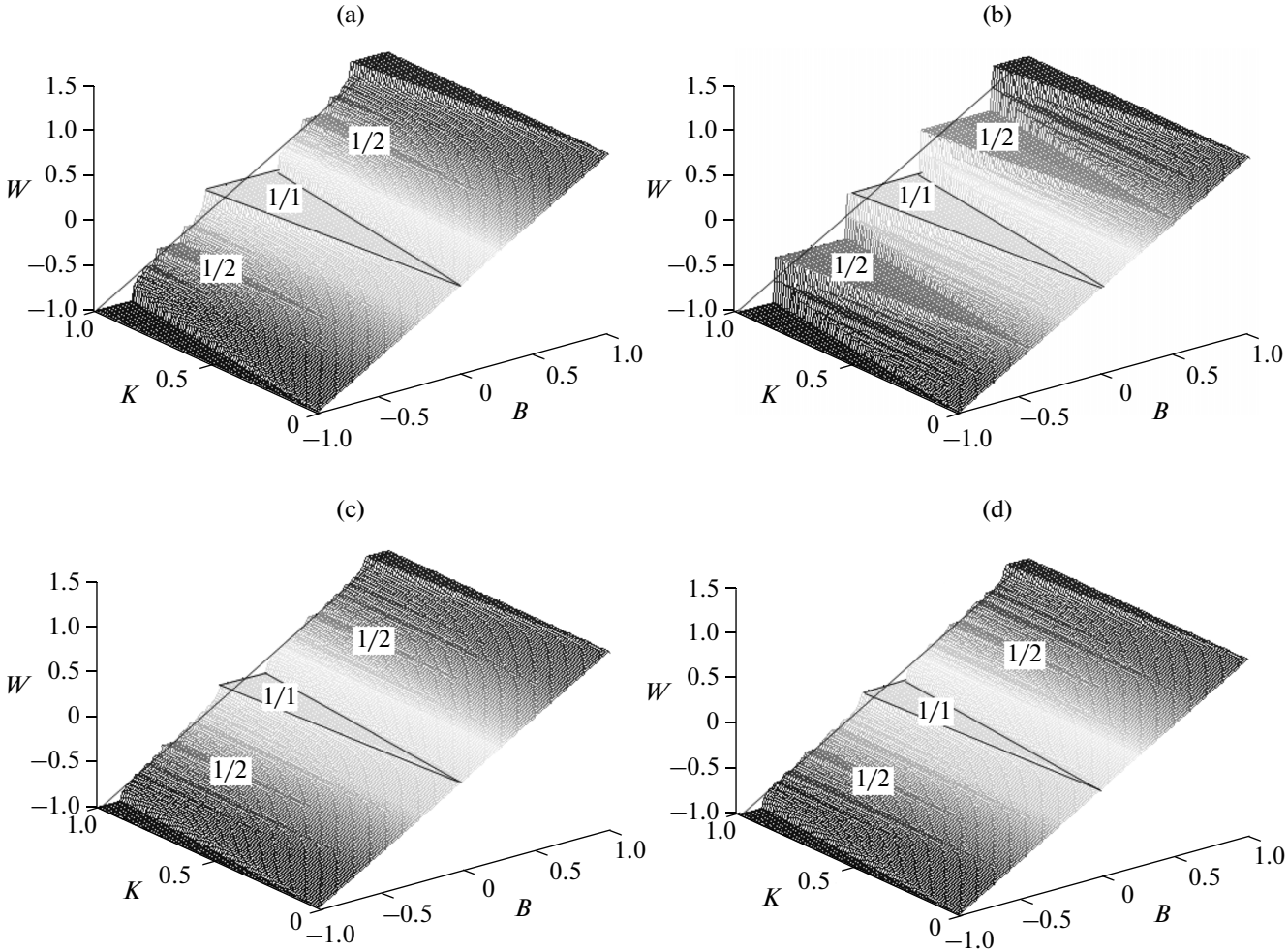

Fig. 20. Plots of rotation number W vs. control parameters K and B.

of control parameters K and B for input signals $F_{1\text{–}5}[x]$ in wide ranges for $K < 4$. The physical maps of the synchronism zones for $F_{1,2}[x]$ are poorer with respect to different types of motion. The synchronization is absent at $K > 2$ in the 1/1, 1/2, 1/3, and 2/3 regimes. The analysis of Figs. 20 and 21 shows that the waveform of the input signal substantially affects the synchronous and asynchronous zones depending on control parameters. For example, a variation in the waveform may lead to the broadening of the working range in the needed interval of variations in the main physical parameters (which is observed for the *Kup* and $Kfup_n$ signals). For $K > 1$, we obtain a complicated physical scenario with overlapped zones of synchronous regimes for atomic input signals (as distinct from the $F_{1,2}[x]$ signals). The overlapped physical zones on the map of control parameters indicate that PLSs can generate chaotic oscillations.

Thus, the sampling PLSs with the *Kup* and $Kfup_n$ signals can used to generate chaotic oscillations. Below, we analyze the dynamic processes inside the zones of synchronism in the vicinity of the corresponding boundaries.

3.4. Effect of Nonuniformity of the Input-Signal Sample on the Spectral Components of the Generated Oscillations

A significant feature of the sampling PLSs lies in the distribution nonuniformity of the samples of input signal on the time axis inside the zones of synchronism. We consider the physical zones in which the effect is manifested and the corresponding consequences. This raises the question of whether the nonuniformity of the sample is manifested in the physical zone with a multiplicity of 1 : 1. As was demonstrated, the TO oscillations are synchronized with the input signal after the transient process in such a way that the $1T$ cycle is established (one sample per one period of the signal). In this case, we have $x_n = x_{n+1} = x_{n+2} = \hat{x}$ starting from a certain n. Thus, coordinate difference $\Delta x = x_{n+1} - x_n$ is zero or 2π and the exact tuning to the

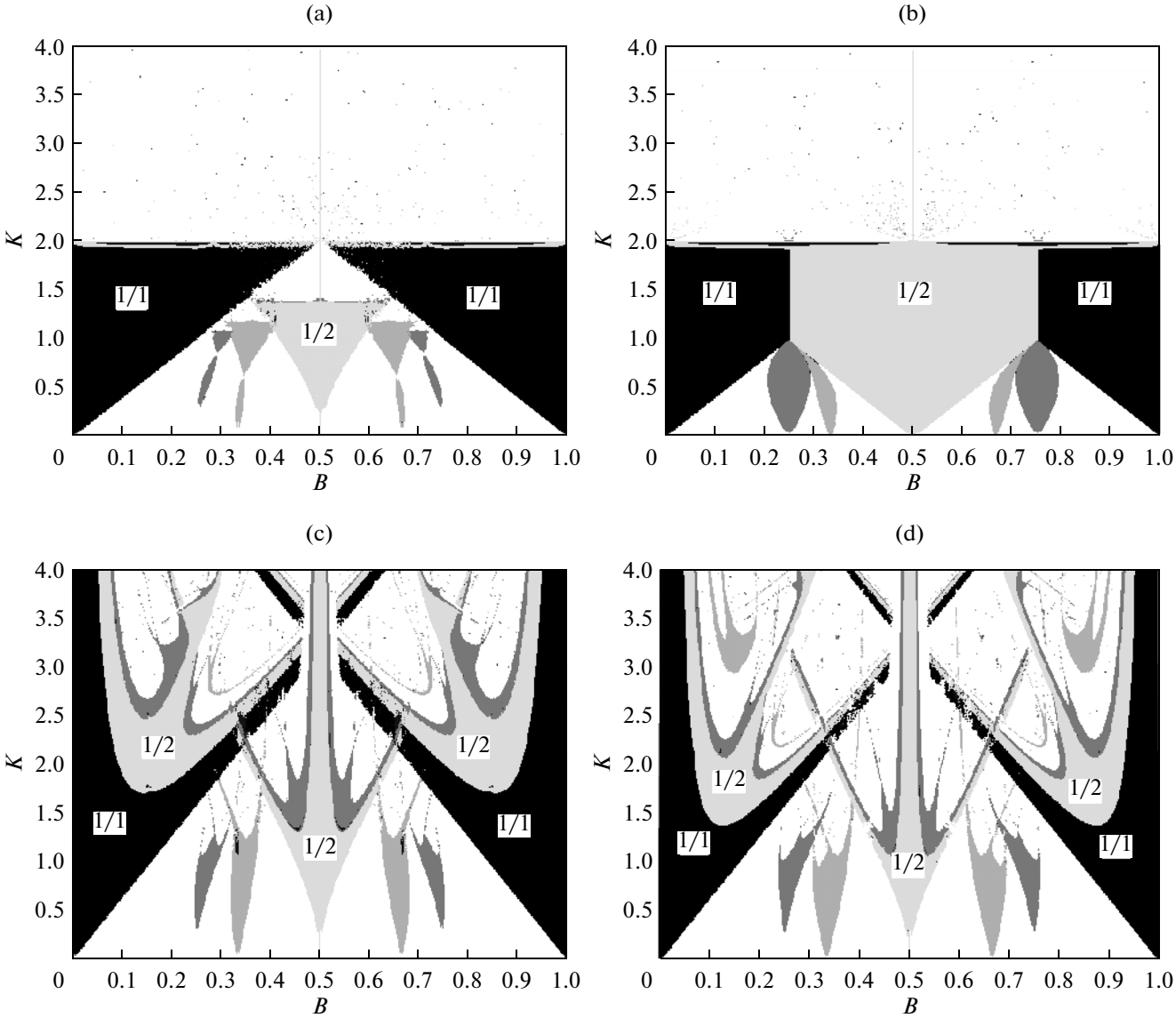

Fig. 21. Physical maps of the zones of synchronous regimes for different waveforms of input signals.

frequency of the input signal takes place in the absence of nonuniformity. Hence, the nonuniformity is manifested only in the physical zones with higher (greater than unity) multiplicity.

We consider the frequency doubling for the working regime in the physical zone of synchronism with a multiplicity of 1/2. Figures 22a and 22b show the oscillograms of the input signals and the generated oscillations of the sampling PLSs in the vicinity of the corresponding boundary. In Fig. 22a ($B = 0.52$), the difference of oscillation periods T_1 and T_2 is insignificant but period T_1 becomes greater than period T_2 in the vicinity of the boundary of the synchronism zone when parameter B increases. The distribution nonuniformity of the samples of input signal increases when we approach the boundary of the physical zone of frequency doubling. A similar scenario is obtained for the physical zones with higher multiplicity. For example, Fig. 23 presents the input and output signals in the zone of frequency tripling. Here, intervals T_1, T_2, and T_3 substantially differ from each other. A similar scenario is obtained for the physical zones with higher multiplicity.

Spurious spectral components at combination frequencies emerge in the spectra of generated oscillations in the physical zones of synchronous regimes with fractional multiplicity in the case of nonuniform sampling of the input signal. The sampling PLSs can hardly be used for the synthesis of high-precision oscillations. A spectral approach to the analysis of

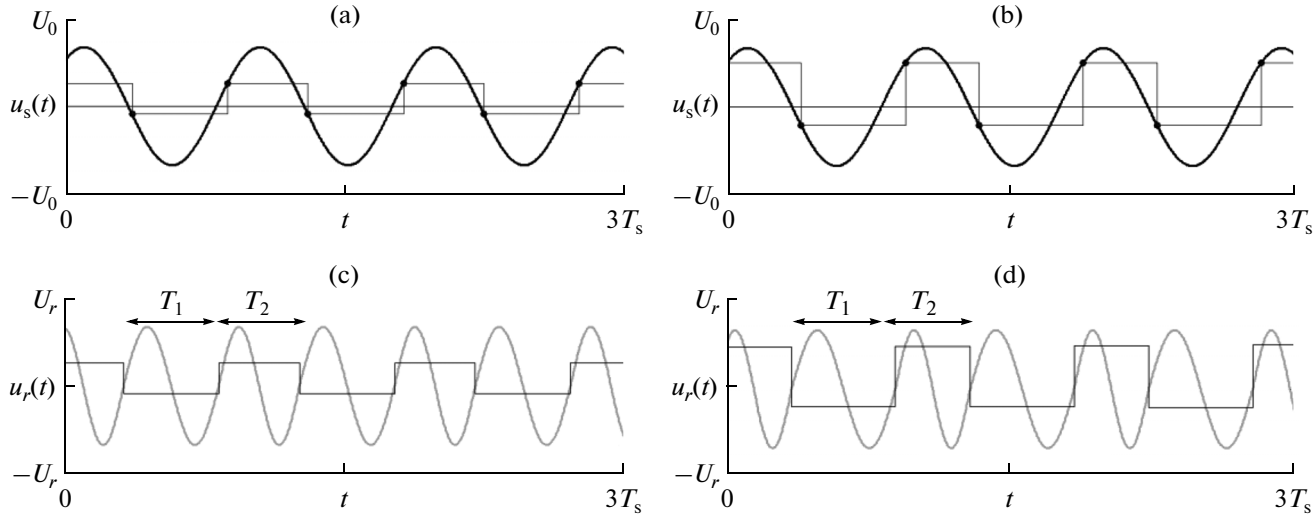

Fig. 22. (a) and (b) Input signals and (c) and (d) output oscillations of the sampling PLS in the vicinity of the boundary of the 1/2-synchronism zone at $B =$ (a) and (c) 0.52 and (b) and (d) 0.53.

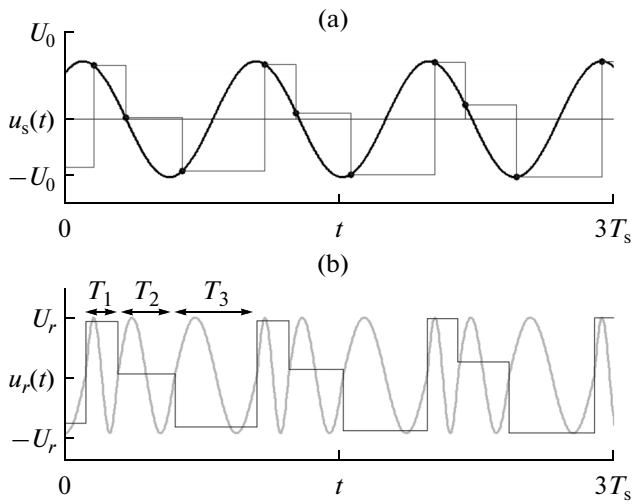

Fig. 23. (a) Input signal and (b) output oscillations of the sampling PLS in the vicinity of the boundary of the 1/3-synchronism zone at $B = 0.34$.

oscillations in the physical zones of synchronous regimes of sampling PLSs needs to be further investigated in additional study.

ACKNOWLEDGMENTS

This study was supported by the Russian Foundation for Basic Research, project no. 13-02-12065.

REFERENCES

1. V. F. Kravchenko, O. V. Kravchenko, V. I. Pustovoit, and D. V. Churikov, J. Commun. Technol. Electron. **59**, 981–1009 (2014).
2. V. F. Kravchenko, O. V. Kravchenko, V. I. Pustovoit, D. V. Churikov, and A. V. Yurin, J. Commun. Technol. Electron. **60**, 109 (2015).
3. V. F. Kravchenko, V. A. Rvachev, and V. L. Rvachev, Radiotekh. Elektron. (Moscow) **40**, 1385 (1995).
4. E. G. Zelkin and V. F. Kravchenko, J. Commun. Technol. Electron. **46**, 829 (2001).
5. V. F. Kravchenko, *Lectures on the Theory and Applications of Atomic Functions* (Radiotekhnika, Moscow, 2003) [in Russian].
6. V. F. Kravchenko and V. L. Rvachev, *Boolean Algebra, Atomic Functions and Wavelets in Physical Applications* (Fizmatlit, Moscow, 2006) [in Russian].
7. *Digital Signal and Image Processing in Radio Physical Applications*, Ed. by V. F. Kravchenko (Fizmatlit, Moscow, 2007) [in Russian].

8. V. K. Volosyuk and V. F. Kravchenko, *Statistical Theory of Radio Systems of Remote Sensing and Radar*, Ed. by V. F. Kravchenko (Fizmatlit, Moscow, 2008) [in Russian].
9. V. F. Kravchenko, H. M. Perez-Meana, and V. I. Ponomaryov, *Adaptive Digital Processing of Multidimensional Signals with Applications* (Fizmatlit, Moscow, 2009).
10. V. F. Kravchenko, O. S. Labun'ko, A. M. Lerer, and G. P. Sinyavskii, *Computational Methods in Modern Radio Physics* (Fizmatlit, Moscow, 2009) [in Russian].
11. A. V. Totsky, A. A. Zelensky, and V. F. Kravchenko, *Bispectral Methods of Signal Processing. Applications in Radar, Telecommunications and Digital Image Restoration* (Walter de Gruyter, Berlin, 2014).
12. V. F. Kravchenko, in *Proc. Int. Conf. on Antenna Theory and Techniques, Lviv, Ukraine, Oct. 6–9, 2009* (Lviv. Politechnic Nat. Univ., Lviv, 2009), p. 3.
13. V. F. Kravchenko, O. V. Kravchenko, V. I. Pustovoit, and D. V. Churikov, Fiz. Osnovy Priborostroen., Spec. Iss. (Nov.), 3 (2011).
14. V. F. Kravchenko, O. V. Kravchenko, V. I. Pustovoit, and D. V. Churikov, Elektromagn. Volny Elektron. Sist. **16** (9), 7 (2011).
15. V. F. Kravchenko, O. V. Kravchenko, V. I. Pustovoit, and D. V. Churikov, in *Proc. 67th Sci. Session of the Popov Society Dedicated to the Radio Day, Moscow, May 16–17, 2012* (RNTORES im. A. S. Popova, Moscow, 2012), pp. III–VIII.
16. *Polynomial Atomic Functions for Fourier Analysis* http://demonstrations.wolfram.com/PolynomialAtomicFunctionsForFourierAnalysis/
17. F. J. Harris, Proc. IEEE **66**, 51 (1978).
18. I. M. Gel'fand, D. A. Raikov, and G. E. Shilov, *Commutative Normalized Rings* (Fizmatlit, Moscow, 2011) [in Russian].
19. V. F. Kravchenko and Ya. Yu. Konovalov, in *Acousto-optical and Radar Methods for Measurements and Information Processing (Proc. 5nd Int. Conf., Suzdal', Russia, Sept. 18–19, 2011)* (NTORES im. A. S. Popova, Moscow, 2012), p. 9.
20. Ya. Yu. Konovalov, in *Proc. 67th Sci. Session of the Popov Society Dedicated to the Radio Day, Moscow, May 16–17, 2012* (RNTORES im. A. S. Popova, Moscow, 2012), p. 103.
21. Ya. Yu. Konovalov, in *Proc. Int. Conf. Days on Diffraction-2012, St. Petersburg, May 28–June 1, 2012* (St. Petersburg Gos. Univ., St. Petersburg, 2012), p. 129.
22. V. F. Kravchenko and Ya. Yu. Konovalov, in *Proc. Int. Conf. Days on Diffraction-2013, St. Petersburg, May 27–31, 2013* (St. Petersburg Gos. Univ., St. Petersburg, 2013), p. 78.
23. V. F. Kravchenko and Ya. Yu. Konovalov, in *Acousto-optical and Radar Methods for Measurements and Information Processing (Collected Papers 5nd Int. Conf., Suzdal', Russia, Sept. 18–19, 2012)* (NTORES im. A.S. Popova, Moscow, 2012), p. 9.
24. Ya. Yu. Konovalov and O. V. Kravchenko, in *Proc. Int. Conf. Days on Diffraction-2014, St. Petersburg, May 26–30, 2014* (St. Petersburg Gos. Univ., St. Petersburg, 2014), p. 132.
25. V. F. Kravchenko and Ya. Yu. Konovalov, in *Acousto-optical and Radar Methods for Measurements and Information Processing (Proc. 7th Int. Conf., Suzdal', Russia, Sept. 15–17, 2014)* (NTORES im. A. S. Popova, Moscow, 2012), p. 132.
26. V. F. Kravchenko, O. V. Kravchenko, and A. R. Safin, Usp. Sovr. Radioelektron., No. 5, 23 (2009).
27. V. F. Kravchenko, O. V. Kravchenko, and A. R. Safin, in *Proc. NTORES im. A. S. Popov*, Ser.: *Acoustooptical and Radar Methods for Metrology and Information Processing*, Vol. 3*: Int. Conf., Suzdal', Russia, Sept. 22–24, 2009* (NTORES im. A. S. Popov, Moscow, 2009), p. 179.
28. V. F. Kravchenko, O. V. Kravchenko, A. R. Safin, and D. V. Churikov, in *Proc. NTORES im. A. S. Popov*, Ser.: *Acoustooptical and Radar Methods for Metrology and Information Processing*, Vol. 3: *Int. Conf., Suzdal', Russia, Sept. 22–24, 2009* (NTORES im. A. S. Popov, Moscow, 2009) p. 9.
29. V. F. Kravchenko, V. I. Pustovoit, and D. V. Churikov, Dokl. Phys. **56**, 471 (2011).
30. V. F. Kravchenko, V. I. Pustovoit, and D. V. Churikov, Elektromagn. Volny Elektron. Sist. **16** (8), 44 (2011).
31. V. F. Kravchenko and D. V. Churikov, in *Digital Signal Processing and Its Applications (Proc. 13th Int. Conf. Moscow, 2011)* (Insvyaz'izdat, Moscow, 2011), Vol. 1, p. 163.
32. V. F. Kravchenko and D. V. Churikov, in *Proc. Int. Conf. Days on Diffraction-2011, St. Petersburg, Russia, May 30–June 3, 2011* (St. Petersburg Gos. Univ., St. Petersburg, 2013), p. 78.
33. V. F. Kravchenko and D. V. Churikov, in *Proc. 67th Sci. Session of the Popov Society Dedicated to the Radio Day, Moscow, May 16–17, 2012* (RNTORES im. A.S. Popova, Moscow, 2012), p. 83.
34. V. F. Kravchenko and D. V. Churikov, in *Proc. Int. Conf. Days on Diffraction-2012, St. Petersburg, May 28–June 1, 2012* (St. Petersburg Gos. Univ., St. Petersburg, 2012), p. 152.
35. V. F. Kravchenko, Ya. Yu. Konovalov, and D. V. Churikov, in *Proc. Progress in Electromagnetics Research Symposium, Aug. 19–23, 2012* (Electromagnetics Academy, Moscow, 2012).
36. V. F. Kravchenko and D. V. Churikov, J. Meas. Sci. Instrum. **4**, 231 (2013).
37. V. F. Kravchenko, O. V. Kravchenko, and A. R. Safin, Elektromagn. Volny Elektron. Sist. **15** (7), 41 (2010).
38. V. F. Kravchenko, O. V. Kravchenko, and A. R. Safin, in *Digital Signal Processing and Its Applications (Proc. 12th Int. Conf. & Exhibition, Moscow, 2010)* (Insvyaz'izdat, Moscow, 2010), Vol. 1, p. 131.
39. M. V. Kapranov, V. F. Kravchenko, O. V. Kravchenko, and A. R. Safin, in *Proc. 2010 Int. Kharkov Symp. on Physics and Engineering of Microwaves, Millimeter and Submillimeter Waves (MSMW'10), Session H: R-Functions, Atomic Functions, Wavelets, Fractals, Kharkov, Ukraine, June 21–26, 2010* (IEEE, New York, 2001), H-7. (3 p.)
40. V. F. Kravchenko, O. V. Kravchenko, and A. R. Safin, in *Proc. Ultrawideband and Ultrashort Impulse Signals, Sevastopol, Sept. 6–10, 2010* (IEEE, New York, 2010), p. 22.

Translated by A. Chikishev